HAL open science

Bidimensional lamellar assembly by coordination of peptidic homopolymers to platinum nanoparticles

Ghada Manai, Hend Houimel, Mathilde Rigoulet, Angélique Gillet, Pier-Francesco Fazzini, Alfonso Ibarra, Stéphanie Balor, Pierre Roblin, Jérôme Esvan, Yannick Coppel, et al.

To cite this version:

Ghada Manai, Hend Houimel, Mathilde Rigoulet, Angélique Gillet, Pier-Francesco Fazzini, et al.. Bidimensional lamellar assembly by coordination of peptidic homopolymers to platinum nanoparticles. Nature Communications, 2020, 11, pp.2051. 10.1038/s41467-020-15810-y . hal-02612552v2

HAL Id: hal-02612552

https://hal.science/hal-02612552v2

Submitted on 11 Jun 2020

HAL is a multi-disciplinary open access archive for the deposit and dissemination of scientific research documents, whether they are published or not. The documents may come from teaching and research institutions in France or abroad, or from public or private research centers.

L'archive ouverte pluridisciplinaire **HAL**, est destinée au dépôt et à la diffusion de documents scientifiques de niveau recherche, publiés ou non, émanant des établissements d'enseignement et de recherche français ou étrangers, des laboratoires publics ou privés.

Distributed under a Creative Commons Attribution 4.0 International License

nature COMMUNICATIONS

ARTICLE

https://doi.org/10.1038/s41467-020-15810-y OPEN

Bidimensional lamellar assembly by coordination of peptidic homopolymers to platinum nanoparticles

Ghada Manai[1,2,8], Hend Houimel[1,8], Mathilde Rigoulet[1], Angélique Gillet[1], Pier-Francesco Fazzini[1], Alfonso Ibarra[3], Stéphanie Balor[4], Pierre Roblin[5], Jérôme Esvan[6], Yannick Coppel[2], Bruno Chaudret[1], Colin Bonduelle[2,7]✉ & Simon Tricard[1]✉

A key challenge for designing hybrid materials is the development of chemical tools to control the organization of inorganic nanoobjects at low scales, from mesoscopic (~μm) to nanometric (~nm). So far, the most efficient strategy to align assemblies of nanoparticles consists in a bottom-up approach by decorating block copolymer lamellae with nanoobjects. This well accomplished procedure is nonetheless limited by the thermodynamic constraints that govern copolymer assembly, the entropy of mixing as described by the Flory–Huggins solution theory supplemented by the critical influence of the volume fraction of the block components. Here we show that a completely different approach can lead to tunable 2D lamellar organization of nanoparticles with homopolymers only, on condition that few elementary rules are respected: 1) the polymer spontaneously allows a structural preorganization, 2) the polymer owns functional groups that interact with the nanoparticle surface, 3) the nanoparticles show a surface accessible for coordination.

[1] Laboratoire de Physique et Chimie des Nano-Objets, INSA, CNRS, Université de Toulouse, Toulouse, France. [2] Laboratoire de Chimie de Coordination, CNRS, Université de Toulouse, Toulouse, France. [3] Instituto de Nanociencia de Aragón, Universidad de Zaragoza, Zaragoza, Spain. [4] Plateforme de Microscopie Électronique Intégrative, Centre de Biologie Intégrative, CNRS, Université de Toulouse, Toulouse, France. [5] Laboratoire de Génie Chimique, Fédération Fermat, INPT, CNRS, Université de Toulouse, Toulouse, France. [6] Institut Carnot – Centre Inter-universitaire de Recherche et d'Ingénierie des Matériaux, INP-ENSIACET, CNRS, Université de Toulouse, Toulouse, France. [7] Laboratoire de Chimie des Polymères Organiques, Université de Bordeaux, CNRS, Bordeaux INP, Pessac, France. [8] These authors contributed equally: Ghada Manai, Hend Houimel. ✉email: colin.bonduelle@enscbp.fr; tricard@insa-toulouse.fr

Structuring hybrid materials combining metallic nanoparticles (NPs) and polymers has stimulated a large effort to make new physical properties emerging: optical, electronic, or magnetic[1–3]. Such composites have the potential of improving the functionality of devices ranging from memory storage to sensors or microelectronic systems[4,5]. In addition, the structural properties of the polymer matrix can give added value to the hybrid materials, such as stimuli-responsiveness[6] or chirality[7]. Among a variety of possible structuring, disposing NPs in lines on substrates paves a way toward anisotropic ordering of matter at the nanoscale, which can be observed, manipulated, and connected. To reach such a supraparticular organization, the most efficient strategy developed so far consists in decorating diblock copolymer lamellar assemblies by NPs, tuning the strength and the nature of weak interactions between the two components (essentially Van de Waals interactions)[5–11]. Diblock copolymer templating is a robust and versatile approach that has been extended to thermal evaporation[12], atomic layer deposition[13], or for structuring molecules such as polyoxometallates[14]. The obtained morphologies are driven by (1) the entropy of mixing of the two blocks, described by the Flory–Huggins solution theory[15,16], and (2) their corresponding volume fractions[17], taking into account that, in presence of NPs, there is a significant decrease in the copolymers' conformational entropy coming from particle sequestration[10]. Although very promising in many situations, the diblock copolymer approach shows important limitations: (1) a constrained size ratio between the two blocks to access lamellar assemblies (generally comprised between 0.4 and 0.6 volume fraction with random coil polymers), (2) in presence of NPs, an imprecise control of their localization (as it is governed by entropy) and (3) in solution, a strong dependence to experimental conditions (concentration, temperature, presence of co-solvent, etc.)[10,15,16]. Here, we present an alternative strategy to dispose NPs in lines by simply mixing metallic ultra-small NPs with structured peptidic homopolymers. The coordination bonding between the polymer functional groups and the NP surface indeed affords lamellar organization, where the patterning distances are linearly controlled by the molecular weight of the polymer.

Self-assembly is a widely applied strategy for preparing various materials based on metallic NPs, which lead to e.g., innovative photonic materials, new microelectronic devices, or structured templates for nanolithography[1]. NPs are generally obtained by a chemical approach that consists in constraining the growth of the crystal by the presence of a limiting agent (ligand, polymer, etc.). An elegant approach resides in decomposing organometallic precursors in mild conditions to obtain clean NPs, i.e. having a surface composition perfectly described and controllable. In this work, we choose, as a standard, ultra-small (<2 nm) platinum NPs, as their sizes are in the same range as the one of a monomer moiety and their surfaces are only stabilized by carbon monoxide (CO) and labile tetrahydrofuran (THF)[18]. The absence of strong organic ligands gives the opportunity to fully describe the coordination between the additional component, *i.e.* the polypeptide polymer, and the NP surface. So far, most approaches involving NPs consider their assemblies as a packing of hard spheres, but the ligand itself has emerged as a chemical leverage, which enables exquisite control to promote supraparticular chemistry[19,20]. Polypeptide polymers are simple macromolecules in which an amino-acid moiety is repeated many times. They adopt ordered secondary conformations such as α-helices or β-sheets, which offer a way to guide structuration at the nanoscale through intermolecular and/or intramolecular interactions[21,22]. In this work, we choose poly(γ-benzyl-*L*-glutamate) (PBLG), a synthetic polypeptide that gives rise to a rigid rod-like α-helical conformation in organic solvents and that has often been employed as a model system to drive lamellar morphologies, when included in block copolymer structures[23].

Results

Description of the nanostructuration. The NPs were synthesized by decomposition of $Pt_2(dba)_3$ (dba = dibenzylideneacetone) under a CO atmosphere in THF, followed by complete elimination of the organic dba residue by washing with pentane[18]. TEM pictures showed well-dispersed NPs, with diameters of 1.2 ± 0.3 nm (Fig. 1a). On another hand, PBLG was synthesized by initiating the ring-opening polymerization of γ-benzyl-*L*-glutamate-*N*-carboxyanhydride with propargylamine in dimethylformamide (Supplementary Fig. 1)[24]. A library of PBLGs spanning a wide range of molecular weights were obtained (Fig. 1b), with five degrees of polymerization (Dp), as measured by ^{1}H NMR and SEC chromatography (Supplementary Table 1): **PBLG1** presented a Dp of 28, **PBLG2** of 69, **PBLG3** of 120, **PBLG 4** of 217, and **PBLG 5** of 481. Their α-helix secondary structures were confirmed by circular dichroism measurements in THF (Fig. 1c and

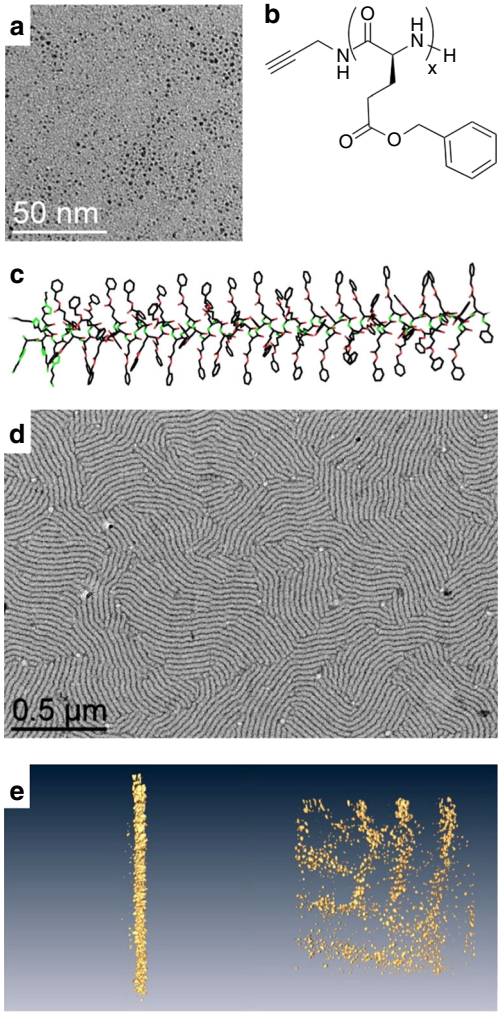

Fig. 1 Building blocks and self-assembly. a TEM image of pristine ultra-small platinum nanoparticles of 1.2 ± 0.3 nm. **b** Chemical structure of PBLG —in the present study, $x = 28$ (**PBLG1**), 69 (**PBLG2**), 120 (**PBLG3**), 217 (**PBLG4**), 481 (**PBLG5**). **c** Geometrical model of the α-helix conformation of PBLG (example for $x = 60$). Lamellar structuration of an assembly of platinum nanoparticles with **PBLG4** at 0.5 eq.: **d** Low-magnification TEM image; **e**, Tomographv 3D reconstruction at two viewing directions: each yellow dot corresponds to an individual nanoparticle.

Supplementary Fig. 2). The assembly of NPs and peptidic polymers was carried out in THF: solutions of platinum NPs and of PBLG were mixed and stirred for 2 h at different equivalent numbers (eq. – defined as the ratio between the monomer unit and the platinum atom quantities). Transmission electron microscopy (TEM) on **PBLG4** at 0.5 eq. showed unexpected lamellar assemblies of the hybrid materials (Fig. 1d), alternating zones containing (dark), or excluding (white) NPs. Such an organization has been observed on both silicon substrates and TEM grids by different microscopy techniques: atomic force microscopy and scanning electron microscopy, in addition to TEM (Supplementary Fig. 3a–c). Tomography imaging showed that the NPs constitute cylindrical lamellae, without any preferential arrangement within each lamella (Fig. 1e and Supplementary Fig. 3d, e). As we did not notice any effect of deposition substrate (hydrophobic carbon vs. hydrophilic silicon), nor of deposition process (drop-casting vs. spin-coating), we hypothesized that these structured lamellae were present in solution and did not form during the solvent evaporation. The existence of the structured lamellae in solution was then confirmed by cryo-TEM imaging, as a same morphology was observed after a fast freezing of the assembly solution (Supplementary Fig. 4). Besides, in some cases, we noticed the presence Moiré patterns, resulting from the superimposition of up to four lamellae (Supplementary Fig. 5). As the lamellae structures are preformed in solution, they can deposit on top of each other during the drop casting of the TEM grid preparation. Such observations gave insight that the system organized in a lamellae-within-lamellae hierarchical assembly[25]. Information on the polymer structure before and after assembly was first given by ^{13}C HR-MAS NMR at slow speed (Supplementary Fig. 6). After NP addition, an increase of the spinning sideband intensities, due to stronger chemical shift anisotropies, highlighted a stiffening of the PBLG in the assembly, which also led to greater conformational homogeneity, as evidenced by the resonance sharpening. Second, SAXS measurements showed a broad peak centered at 0.25 Å^{-1} (Supplementary Fig. 7), meaning that NPs were separated from each other by an average correlation distance equal to 2.5 nm. The importance of the ratio between the monomer unit and the platinum atom quantities was then studied by varying the eq. number from 0.05 up to 5 eq. with **PBLG4**. Without any polymer, the NPs simply aggregated because of the capillary forces generated by THF evaporation (Fig. 2a), without showing any specific average distance by SAXS analysis (Supplementary Fig. 7). As soon as PBLG was added to the reaction mixture, depletion zones without NPs formed (Fig. 2b–d), attributed to the presence of the polymer. Very clean patterns were obtained at 0.5 eq, with alternation of regular lamellae. At higher ratios, this NP organization became looser (1 eq.—Fig. 2d), and totally disappeared at 5 eq. (Supplementary Fig. 8). A window of two orders of magnitude in eq. number (from 0.05 to 5 eq.) was thus accessible to tune the pattern structure of the lamellar assemblies.

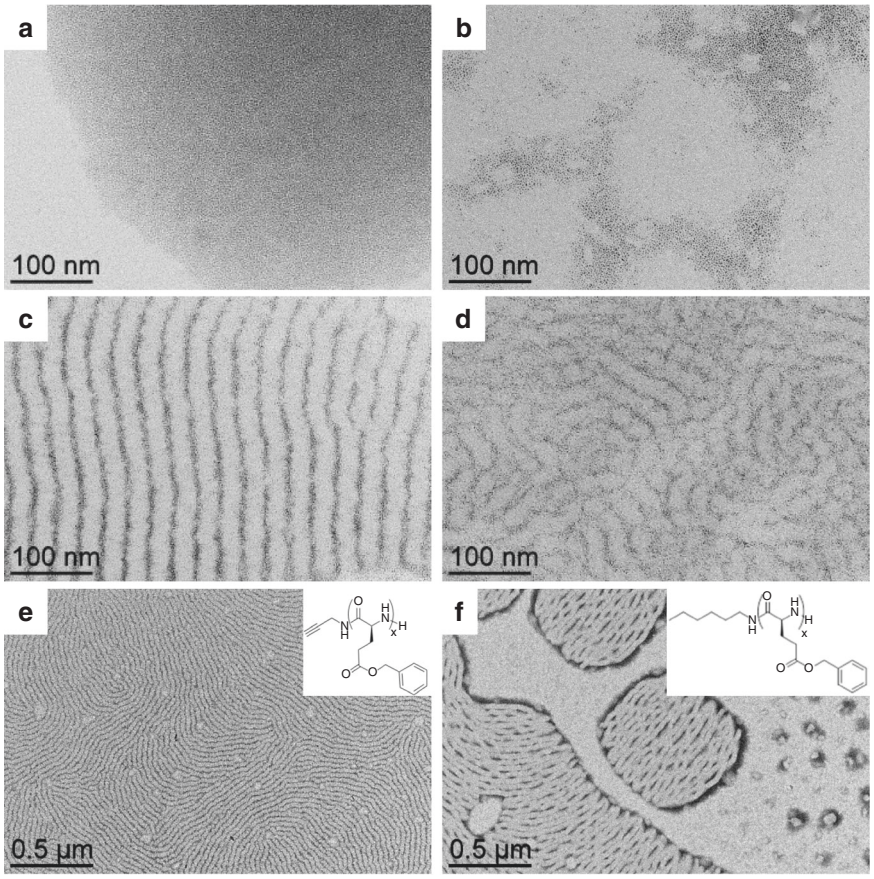

Fig. 2 Effect of the relative quantity of polymer vs. nanoparticle and effect of the terminal group. TEM micrographs of the assemblies after 2 h of reaction between platinum nanoparticles and: **PBLG4** at **a** 0 eq. (nanoparticles alone); **b** 0.05 eq.; **c** 0.5 eq.; **d** 1 eq. (an equivalent eq. refers to the number of introduced monomers per platinum atom). The assembly process occurs at an optimum relative ratio of polymer vs. nanoparticle equal to 0.5 eq. TEM micrograph of the assemblies between platinum nanoparticles and: **e PBLG4**; **f PBLG-H**, at 0.5 eq., after 2 h of reaction. Insets represent the chemical structures of the polymers. The nature of the terminal group of PBLG influences the global cohesion of the hybrid system, as alkyne groups lead to better structuration than hexyl groups.

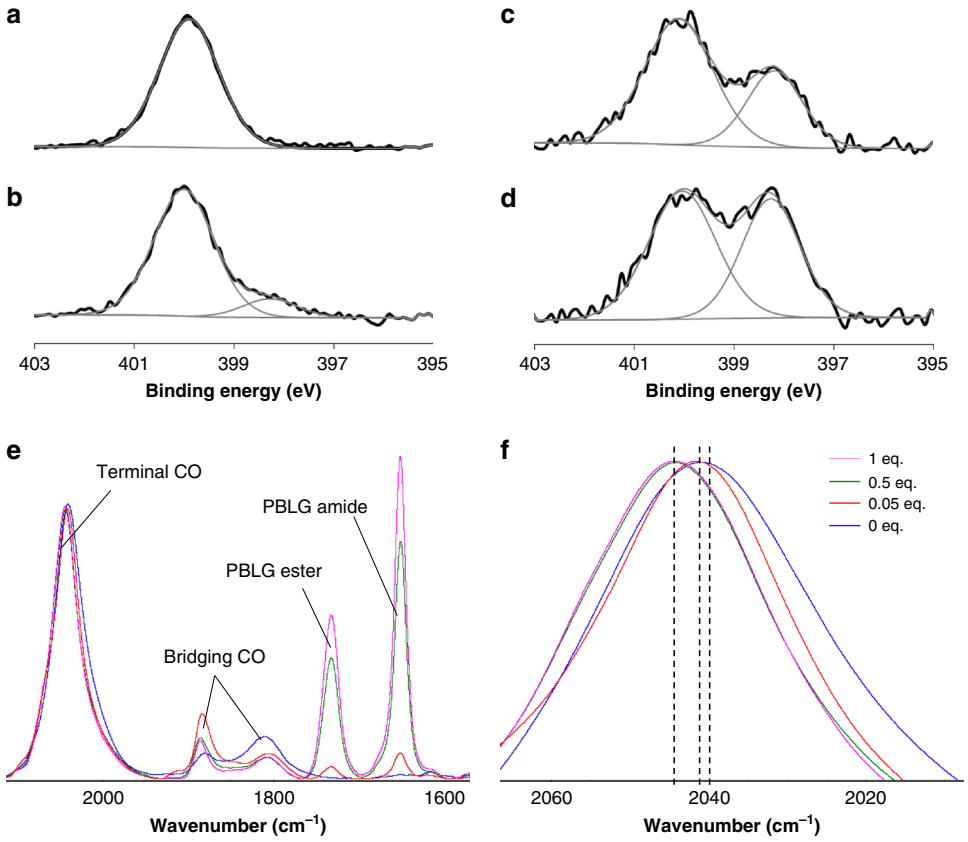

Fig. 3 Spectroscopic signature of coordination of the peptidic polymer to the nanoparticle surface. a XPS spectrum at the N*1s* edge of **PBLG4** alone. XPS spectra at the N*1s* edge of assemblies between platinum nanoparticles and **PBLG4** at: **b** 1 eq. (12% of component at 398 eV); **c** 0.5 eq. (33% of component at 398 eV); **d** 0.05 eq. (45% of component at 398 eV). **e** Infrared spectra of CO coordinated at the nanoparticle surface and of peptide bond of the polymer within the assemblies (at 0 eq., 0.05 eq., 0.5 eq., and 1 eq.). The spectra are normalized to the signal of the CO vibration around 2040 cm^{-1}. **f** Zoom on the infrared spectra of Fig. 2e at the terminal CO region. The assembly process is characterized by a specific signature both in XPS and infrared spectroscopies.

Origin of the patterning. To determine key parameters at the origin of the patterning, coordination of the polymer to the NP surface was studied. First, a peptidic dimer **DBLG** was specifically prepared and mixed with NPs to confirm the possible coordination of the alkyne moiety at the NP surface. ^{13}C solid-state MAS NMR showed the disappearance of the peaks at 72 and 80 ppm attributable to the alkyne moiety upon NP addition, whereas the other peaks of the molecule remained unchanged (Supplementary Fig. 9). This disappearance strongly supported the occurrence of similar alkyne coordination to the NP surface with **PBLG4**. A polymeric analogue without alkyne was then synthesized from hexylamine, **PBLG-H**. After mixing with NPs, TEM imaging showed a significantly less structured system, with free NPs and more discontinuous NP arrangement within the lamellae (Fig. 2e, f), thus confirming the importance of the alkyne coordination. Second, another coordination bonding between the NP surface and the polymer was identified by X-ray photoelectron spectroscopy (XPS) at the N*1s* edge, which showed the appearance of a new peak at 398 eV in addition to the neutral component at 400 eV of the free polymer. The relative intensity of this peak significantly increased when the eq. number decreased (Fig. 3a–d and Supplementary Fig. 10), confirming a rise of the electronic density on the PBLG amide nitrogen upon NP addition. Simultaneously, both the relative increase of surface platinum oxidation measured by XPS at the Pt*4f* edge (Supplementary Fig. 11), and the progressive shift of the adsorbed CO peak in infrared spectroscopy from 2040 cm^{-1} at 0 eq. to 2041 cm^{-1} at 0.05 eq. and to 2045 cm^{-1} at 0.5 and 1 eq. confirmed a decrease of the electronic density at the NP surface upon PBLG addition (Fig. 3e, f and Supplementary Fig. 12)[18]. Overall, both XPS and infrared measurements reflected an electronic transfer from the NP surface to reduce the PBLG nitrogen in the composite materials, as already observed for amides in platinum molecular complexes[26,27]. The present study thus indicates that the polymer interacts with the NP surface by both coordinating the terminal alkyne group of the polypeptide and its peptide linkages.

Influence of the degree of polymerization. We further explored the Dp influence on the lamellar assemblies. No arrangement was observed with **PBLG1**, but image analysis showed that the width of the lamellae average periodicity regularly increased from **PBLG2** to **PBLG5** (Fig. 4, Supplementary Fig. 13, and Supplementary Table 2). Such a tendency was confirmed by SAXS measurements (Supplementary Fig. 14 and Supplementary Table 2). In addition, the average width of the white zones containing the polymer was equal at any Dp to the length of the PBLG model in α-helices conformation. Similarly, the evolution of the average width of the dark zones containing the NPs as a function of Dp (x) could be fitted by the diameter of gyration of a random coil model $R_g = R_0\ x^{\nu}$. The ν value was fixed to 0.6, as predicted by theory and confirmed by experiments for excluded-volume chains[28]. Extensive study on chemically unfolded proteins found a R_0 value equal to 1.33[28], whereas the fit of our experimental data gave a R_0 value equal to 0.22, thus divided by six. Such a result can be interpreted by the presence of an average of 6–7 bridges within the polymer[29], which is coherent considering the PBLG polymer in a coil disordered state, internally connected

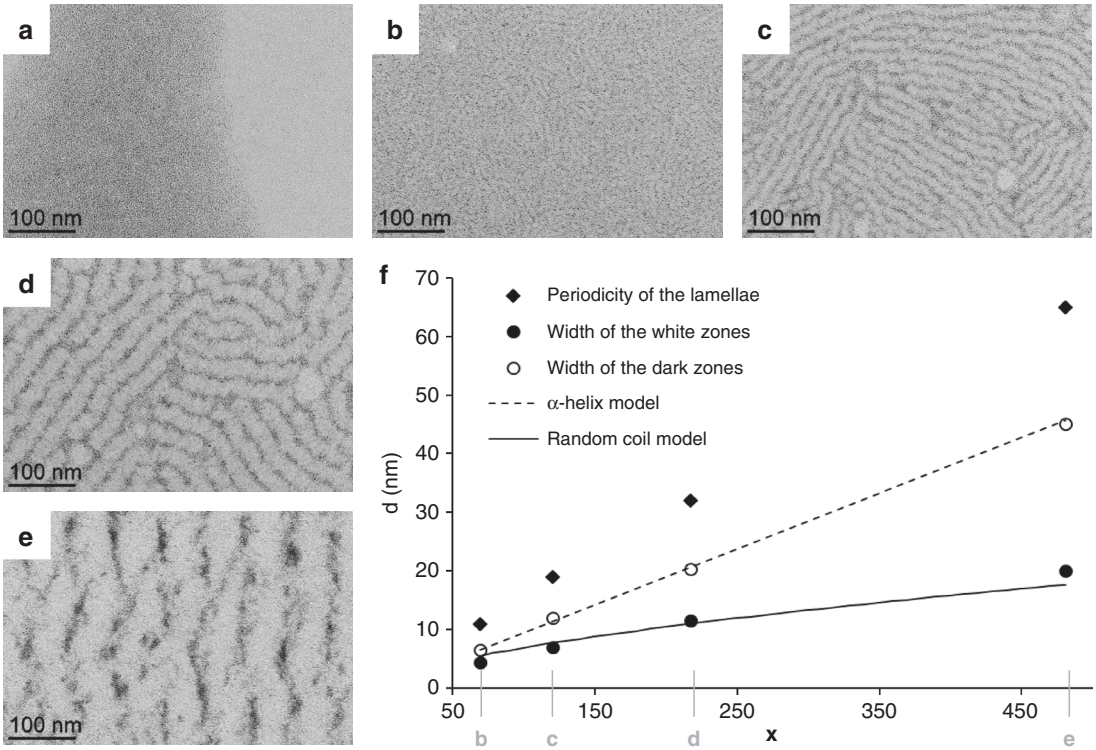

Fig. 4 Effect of the degree of polymerization. TEM micrographs of assemblies between platinum nanoparticles and: **a PBLG1**; **b PBLG2**; **c PBLG3**; **d PBLG4**; and **e PBLG5**. **f**, Evolution of average characteristics as a function of the degree of polymerization x (the α-helix model curve represents the length of the polymer as shown in Fig. 1c for $x = 60$; the random coil model curve represents the diameter of gyration evolution of excluded volume random coil model with $R_0 = 0.22$ and $\nu = 0.6$). Positions corresponding to the micrographs of Fig. 4**b**, **c**, **d**, and **e** are made explicit on the x-axis.

by NP bridges. Analysis of tomography reconstruction confirmed that the thickness of the NP containing zones was comparable to their width (Supplementary Fig. 15). Interpretation of TEM imaging is thus in line with geometrical models where aligned polymers in α-helices alternate with alignments of coiled polymers interacting with NPs. Similar dependence with Dp was obtained if the ratio of polymer number over NP was kept constant (Supplementary Fig. 16, here the eq. number varied from 0.06 to 0.81), confirming the robustness of the patterning to variations of the polymer to NP ratio. Our assembly approach is thus a robust and simple alternative to diblock copolymer templating for structuring metallic NPs. It allows a large patterning period window comprised between 10 and 100 nm, depending on the polypeptide Dp, and can be easily described by simple geometrical models of polymers (α-helices and excluded-volume chains).

First steps of the assembly. In order to give insight on the lamellae formation mechanism, a time dependent study was performed with **PBLG3** and **PBLG4** (Supplementary Fig. 17). Although the standard assembly time was set to 2 h to be sure to reach a steady state (Supplementary Fig. 17a, b), we noticed that the lamellar structure was already present after five seconds, but significantly less advanced (Supplementary Fig. 17c, d). Some free NPs were indeed not assembled and aggregated around the structured zones, and the NPs lamellae were discontinuous. In order to probe effects of a fraction of second of mixing, we first deposited the PBLG on the TEM grid and we added the NP in a second time (Supplementary Fig. 17e, f). We confirmed a pre-structuration of the polymer materials, illustrated by depletion zones without NP, and a beginning of decoration of such zones by the NP, which will then interact with and coordinate to the functional groups of the peptidic polymer.

Discussion

The results of the present study show it is possible (1) to generate anisotropic ordering of platinum NPs in lamellar assemblies by mixing with peptidic homopolymers and (2) to easily tune the dimension of these lamellar assemblies by simply varying the molar mass of the homopolymer. Generally, NP-homopolymer systems do not give extended nanostructured materials but rosaries of NPs that decorate the polymer[30]. Our results can be explained by the fact that PBLG adopt ordered secondary conformation, α-helices, which could spontaneously interact and align with each other following a nematic liquid crystal behavior[23]. The addition of NPs does not result in a simple decoration of the liquid crystal[31,32], and we hypothesized that a destructuring of some of the α-helices occurred thanks to coordination of the peptide linkages with the NP surface (a scheme of the self-assembly process is presented on Supplementary Fig. 18). This NP/polymer association would then drive a small amount of PBLG to adopt a coil-disordered state, where the NPs bridge some part of the polymers. The demixing of the two resulting phases (the NP/coil polymer hybrid on one hand and the aligned α-helices on the other hand) was facilitated by the coordination of the terminal alkyne groups on the NP surface, and led to an anisotropic ordering of NPs. In the future, to ensure optimal performances, rational design of lamellar NP assembly including polymer should consider functional and structured polymers such as peptidic polymers and a fine-tuning of the chemical interaction between the anchoring moieties of the polymers and the NP surface.

Methods

Starting materials. All chemicals were purchased from Sigma-Aldrich and used as received. γ-benzyl-*L*-glutamate N-carboxyanhydride (γ-BLG NCA) was purchased from Isochem. Propargylamine and hexadecylamine were distilled before use. DMF and THF were obtained from a Solvent Purification System and freshly used.

General procedure for the synthesis of PBLGs. The NCA monomer of γ-benzyl-*L*-glutamate (BLG-NCA, 2 g, 7.6 mmol) was weighed in a glovebox under pure argon, introduced in a flame-dried schlenk, and dissolved with 4 mL of anhydrous DMF. The solution was stirred for 10 min, and propargylamine (for instance for **PBLG4**, 2 µL, 0.03 mmol) was added with an argon purged syringe. The solution was stirred for 3 days at room temperature under argon. The polymer was then recovered by precipitation in diethylether and dried under high vacuum, analyzed by ^{1}H NMR ($CDCl_3$ + 15% trifluoroacetic acid). Yield: 81–92%. Molar masses were first determined by ^{1}H NMR using the intensity of methylene protons of the initiator at 3.9 ppm and the intensity of methylene protons of the PBLG at 5.1 ppm. Representative ^{1}H-NMR of the polypeptide backbone (400 MHz, δ, ppm): 2.13 (m, 2H,CH_2), 2.59 (t, 2H, CH_2, $J = 7.09$ Hz), 4.37 (t, 1H, CH, $J = 6.56$ Hz), 5.13 (s, 2H, CH_2O), 6.75 (s, 1H, NH), 7.35 (m, 5H, ArH)[24]. **PBLG1** presented a Dp of 25, **PBLG 2** a Dp of 59, **PBLG3** a Dp of 92, **PBLG 4** a Dp of 171, and **PBLG 5** a Dp of 373 (Supplementary Table 1). **PBLG-H** was synthesized following the same procedure but was initiated by hexylamine instead. Polymer molar masses were determined by SEC using dimethyformamide (DMF + LiBr 1 g L^{-1}) as the eluent. Measurements were performed on an Ultimate 3000 system from Thermoscientific equipped with diode array detector DAD. The system also includes a multi-angles light scattering detector MALS and differential refractive index detector dRI from Wyatt technology. Polymers were separated on three Shodex Asahipack gel columns [GF-1G 7B (7.5 × 8 mm), GF 310 (7.5 × 300 mm), GF510 (7.5 × 300), exclusion limits from 500–300 000 Da] at a flowrate of 0.5 mL min^{-1}. Easivial kit of Polystyrene from Agilent was used as a standard (Mn from 162 to 364,000 Da). Individual offline batch-mode measurements were performed to determine the homopolymers accurate refractive index increments (*dn/dc*) at 50 °C. All the samples (5 mg mL^{-1}) were dissolved in DMF and were run at a flow rate of 0.5 mL min^{-1} at 55 °C: **PBLG1** presented a Dp of 28, **PBLG2** a Dp of 69, **PBLG3** a Dp of 120, **PBLG 4** a Dp of 217, and **PBLG 5** a Dp of 481.

The secondary structure of the PBLG blocks were studied by CD spectroscopy in THF using the following procedure: the final concentration (the concentration in the cuvette used for the CD analyses) was 180 µM in monomer units. The pathlength used was 0.01 mm to decrease the THF UV absorbance and to access correct CD signal down to 200 nm. In these conditions, the CD monitoring was performed in high resolution mode. The molar ellipticity also called the mean residue ellipticity has been calculated as follow: $[\phi] = (10\ q_{obs})/(l \times c)$. $[\phi]$ is expressed in deg cm^2 $dmol^{-1}$. q_{obs} was the observed ellipticity in degrees (deg), l is the path length in dm, and c is the polypeptide concentration in mol L^{-1}. The range from 190 to 250 nm corresponds to the peptide bond absorption. The CD shape of all PBLGs presented two minima at about 208 and 222 nm that were attributable to α-helical structuring (Supplementary Fig. 1 for PBLG4 for which the CD signature of the helix displayed a slightly smaller 208 nm minimum as compared with a 222 nm minimum: $[\phi]$ value of −11.52 mdeg cm^2 $dmol^{-1}$ at 208 nm and −12.59 mdeg cm^2 $dmol^{-1}$ at 222 nm)[22].

Synthesis of DBLG. The NCA monomer of γ-benzyl-*L*-glutamate (BLG-NCA, 2 g, 7.6 mmol) was weighed in a glovebox under pure argon, introduced in a flame-dried schlenk, and dissolved with 6 mL of anhydrous DMF. The solution was stirred for 10 min. at 0 °C, and 1 mL of a DMF solution containing propargylamine (243 µL, 3.8 mmol) was added with an argon purged syringe. The solution was stirred for 3 h at 0 °C under argon. Upon lyophilization, the crude residue was purified by chromatography on silica gel using CH_2Cl_2/MeOH as an eluent. The dimer was isolated as a white solid (54%, 0.9 g).

Synthesis of platinum nanoparticles. The PtNPs have been synthesized as follows[18,33]: all operations were carried out using Fischer–Porter bottle techniques under argon. A solution of $Pt_2(dba)_3$ (90 mg; 0.165 mmol of Pt) in 20 mL of freshly distilled and deoxygenated THF was pressurized in a Fischer–Porter bottle with 1 bar of CO during 30 min at room temperature under vigorous stirring. During this time, the solution color changed from violet to brown (attesting the formation of the NPs). The mixture was evaporated and washed with pentane to eliminate the dba (3 × 20 mL), and to obtain native NPs. The colloid was then redissolved in 20 mL of THF. The size of the NPs was found to be equal to1.2 ± 0.3 nm. For each series of measurements, the sizes were determined by TEM imaging.

Self-assembly. 1 mL of a solution of PBLG polymer in THF (2 mg in 1 mL for 0.50 eq.) was added to 4 mL of the native nanoparticle mixture under vigorous mixing. The precursor concentrations were adapted to obtain the desired equivalent of PBLG monomer per introduced Pt. The brown solution was agitated for 2 h. Drops of the crude solution were deposited on specific substrates for each characterization (see below).

Spectroscopy for PBLG polymers. ^{1}H NMR spectra were recorded on a Bruker AC 400 spectrometer.

For circular dichroism in THF: CD spectra were recorded on a JASCO J-815 Spectropolarimeter between 205 and 260 nm (far-UV), by using a quartz cell of 0.1 cm path length, at 20 °C. The measure parameters were optimized as follows: high sensitivity, between 5 and 20 mdeg, 0.01 mdeg resolution, 8 s response time (digital integration time), 1 nm bandwidth and 5 nm min^{-1} scanning rate.

Microscopy. Samples for TEM were prepared by deposition of one drop of the crude solution on a carbon covered holey copper grid. TEM analyses were performed at the centre de microcaractérisation Raimond Castaing using a JEOL JEM 1400 electron microscope operating at 120 kV. The mean size of the particles and the mean widths of the white and dark zones of the lamellae were determined by image analysis on a large number of objects (~300) using the ImageJ software. The auto-correlation analysis, for determining the average periodicity of the lamellae (shown on Supplementary Fig. 13), has been perform with Gatan DigitalMicrograph software. Low resolution electron tomography has been performed on a JEOL JEM 1400 microscope operated at 120 kV installed in the METI platform in Toulouse. Angles between −60° and 60° with a 2° interval where used for the acquisition. The 3D volume reconstruction has been obtained using the weighted back projection algorithm in IMOD. High resolution STEM HAADF tomography was performed at the Advanced Microscopy Laboratory (LMA), Instituto Universitario de Nanociencia de Aragon (INA), Zaragoza, Spain, by a FEI Tecnai field emission gun operated at 300 kV. 3D reconstruction was carried out with FEI tomography acquisition software, Inspect 3D and Amira 3D reconstruction software after the acquisition of 140 images.

Cryo-TEM has been performed on a JEOL 2100 microscope, equipped with a LaB6 cathode, and operated at 200 kV under low dose conditions. To prepare the samples, 3 µL of sample were deposited onto glow-discharged lacey carbon grids and placed in the thermostatic chamber of a Leica EM-GP automatic plunge freezer, set at 20 °C and low humidity. Excess solution was removed by blotting with Whatman n°1 filter paper for 0.5 s, and the grids were immediately flash frozen in liquid nitrogen. The frozen specimens were placed in a Gatan 626 cryo-holder for imaging. Images were acquired with SerialEM software, with defocus of 1–2 µm, on a Gatan US4000 CCD camera. This device was placed at the end of a GIF Quantum energy filter (Gatan, Inc.), operated in zero-energy-loss mode, with a slit width of 25 eV. Images were recorded at a nominal magnification of 4000 corresponding to calibrated pixel sizes of 1.71 Å.

AFM images were performed with an AIST-NT SmartSPM 1000 microscope. We used silicon tips (Mikromash HQNSC15/ALBS). SEM images were acquired. For both AFM and SEM experiments, the samples were prepared by drop casting of one drop of the crude solution on silicon wafers.

FT-IR spectra were recorded on a Thermo Scientific Nicolet 6700 FT-IR spectrometer in the range 4000–700 cm^{-1}, using a Smart Orbit ATR platform. The sample deposition was performed by drop casting of the crude solution on the germanium crystal of the platform; the measurement was acquired after evaporation of the THF solvent.

Diffraction measurement. X-ray diffraction patterns were recorded on a PANalytical Empyrean diffractometer using the Co Kα radiation. Small angle measurements were performed on a microscopy glass, on which the crude solution was drop-casted. An advantage of working with particles smaller than 2 nm is that the inter-particle distance is sufficiently small to observe correlation distances between two particles with a regular XRD diffractometer without the need of any dedicated SAXS facilities.

Regular Small Angle X-Ray Scattering (SAXS) measurements were performed on a XEUSS 2.0 laboratory source equipped with a pixel detector PILATUS 1 M (DECTRIS) and an X-ray source provided by GeniX3D with a fixed wavelength based on Cu Kα radiation ($\lambda = 1.54$ Å). The sample to detector distance was fixed at 1216.5 mm giving a q range starting from 0.005 to 0.5 $Å^{-1}$ assuming that q is the scattering vector equal to $4\pi/\lambda \sin\theta$ with 2θ the scattering angle. The distance was calibrated in the small angle region using silver behenate (d001 = 58.34 Å). Measurements were performed on samples in solution in capillaries. Concentration of the sample was necessary to observe a signal, so that measurements have been performed on a system that started to precipitate. The capillaries were sealed to prevent solvent evaporation and traces of water, and placed on motorized sample holder. To remove scattering and absorption from air, a primary vacuum has been applied to the entire instrument. Acquisition time per sample was set to 1 h and all scattering curves were corrected for the solvent and capillary contributions, divided by the transmission factor, acquisition time and optical path in order to obtain SAXS curves in absolute units (cm^{-1}).

Spectroscopy. X-Ray Photoelectron Spectroscopy (XPS) analyses were performed at CIRIMAT Laboratory (Toulouse) using a Thermoelectron Kalpha device. The photoelectron emission spectra were recorded using Al-Kα radiation ($h\nu$ = 1486.6 eV) from a monochromatized source. The analyzed area was about 0.15 mm^2. The pass energy was fixed at 40 eV. The spectrometer energy calibration was made using the C1s (284.5 ± 0.1 eV) photoelectron lines. XPS spectra were recorded in direct mode N(Ec). The background signal was removed using the Shirley method. The atomic concentrations were determined from photoelectron peak areas using the atomic sensitivity factors reported by Scofield, taking into account the transmission function of the analyzer. The photoelectron peaks were analyzed by Gaussian/Lorentzian (G/L = 50) peak fitting.

Solid-state NMR experiments were recorded on a Bruker Avance III HD 400 spectrometer equipped with a 4 mm probehead. Samples were wetted with 20 µl of THF-d_8 and spun between 1 and 5 kHz at 293 K. ^{1}H MAS was performed with DEPTH pulse sequence and a relaxation delay of 3 s. For ^{13}C MAS, single

pulse experiments were performed with a recycle delay of 2 s. All chemical shifts for ^{13}C and ^{1}H are relative to TMS.

Data availability

Data are provided in the article or in Supplementary information. Original data are available from the corresponding authors upon reasonable request.

Received: 7 November 2019; Accepted: 25 March 2020;
Published online: 28 April 2020

References

1. Kao, J., Thorkelsson, K., Bai, P., Rancatore, B. J. & Xu, T. Toward functional nanocomposites: taking the best of nanoparticles, polymers, and small molecules. *Chem. Soc. Rev.* **42**, 2654–2678 (2013).
2. Mei, S., Staub, M. & Li, C. Y. Directed nanoparticle assembly through polymer crystallization. *Chem. Eur. J.* **26**, 349–361 (2020).
3. Yi, C., Yang, Y., Liu, B., He, J. & Nie, Z. Polymer-guided assembly of inorganic nanoparticles. *Chem. Soc. Rev.* **49**, 465–508 (2020).
4. Huynh, W. U., Dittmer, J. J. & Alivisatos, A. P. Hybrid nanorod-polymer solar cells. *Science* **295**, 2425–2427 (2002).
5. Balazs, A. C., Emrick, T. & Russell, T. P. Nanoparticle polymer composites: where two small worlds meet. *Science* **314**, 1107–1110 (2006).
6. Zhao, Y. et al. Small-molecule-directed nanoparticle assembly towards stimuli-responsive nanocomposites. *Nat. Mater.* **8**, 979–985 (2009).
7. Sanwaria, S. et al. Helical packing of nanoparticles confined in cylindrical domains of a self-assembled block copolymer structure. *Angew. Chem. Int. Ed.* **53**, 9090–9093 (2014).
8. Lin, Y. et al. Self-directed self-assembly of nanoparticle/copolymer mixtures. *Nature* **434**, 55–59 (2005).
9. Warren, S. C. et al. Ordered mesoporous materials from metal nanoparticle–block copolymer self-assembly. *Science* **320**, 1748–1752 (2008).
10. Haryono, A. & Binder, W. H. Controlled arrangement of nanoparticle arrays in block-copolymer domains. *Small* **2**, 600–611 (2006).
11. Leffler, V. B. et al. Controlled assembly of block copolymer coated nanoparticles in 2D arrays. *Angew. Chem. Int. Ed.* **58**, 8541–8545 (2019).
12. Lopes, W. A. & Jaeger, H. M. Hierarchical self-assembly of metal nanostructures on diblock copolymer scaffolds. *Nature* **414**, 735–738 (2001).
13. Peng, Q., Tseng, Y.-C., Darling, S. B. & Elam, J. W. Nanoscopic patterned materials with tunable dimensions via atomic layer deposition on block copolymers. *Adv. Mater.* **22**, 5129–5133 (2010).
14. Lunkenbein, T. et al. Direct synthesis of inverse hexagonally ordered diblock copolymer/polyoxometalate nanocomposite films. *J. Am. Chem. Soc.* **134**, 12685–12692 (2012).
15. Darling, S. B. Directing the self-assembly of block copolymers. *Prog. Polym. Sci.* **32**, 1152–1204 (2007).
16. Mai, Y. & Eisenberg, A. Self-assembly of block copolymers. *Chem. Soc. Rev.* **41**, 5969–5985 (2012).
17. Jain, S. & Bates, F. S. On the origins of morphological complexity in block copolymer surfactants. *Science* **300**, 460–464 (2003).
18. Tricard, S. et al. Chemical tuning of Coulomb blockade at room-temperature in ultra-small platinum nanoparticle self-assemblies. *Mater. Horiz.* **4**, 487–492 (2017).
19. Nie, Z., Petukhova, A. & Kumacheva, E. Properties and emerging applications of self-assembled structures made from inorganic nanoparticles. *Nat. Nanotechnol.* **5**, 15–25 (2010).
20. Wei, J., Schaeffer, N. & Pileni, M.-P. Ligand exchange governs the crystal structures in binary nanocrystal superlattices. *J. Am. Chem. Soc.* **137**, 14773–14784 (2015).
21. Bellomo, E. G., Wyrsta, M. D., Pakstis, L., Pochan, D. J. & Deming, T. J. Stimuli-responsive polypeptide vesicles by conformation-specific assembly. *Nat. Mater.* **3**, 244–248 (2004).
22. Bonduelle, C. Secondary structures of synthetic polypeptide polymers. *Polym. Chem.* **9**, 1517–1529 (2018).
23. Klok, H.-A., Langenwalter, J. F. & Lecommandoux, S. Self-assembly of peptide-based diblock oligomers. *Macromolecules* **33**, 7819–7826 (2000).
24. Schatz, C., Louguet, S., LeMeins, J. F. & Lecommandoux, S. Polysaccharide-*block* -polypeptide copolymer vesicles: towards synthetic viral capsids. *Angew. Chem. Int. Ed.* **48**, 2572–2575 (2009).
25. Ruokolainen, J. et al. Supramolecular routes to hierarchical structures: comb-coil diblock copolymers organized with two length scales. *Macromolecules* **32**, 1152–1158 (1999).
26. Liang, L.-C., Lin, J.-M. & Lee, W.-Y. Benzene C–H activation by platinum(ii) complexes of bis(2-diphenylphosphinophenyl)amide. *Chem. Commun.* **19**, 2462–2464 (2005).
27. Unger, Y. & Strassner, T. Platinum(II) complexes with amide-functionalized NHC ligands. *J. Organomet. Chem.* **713**, 203–208 (2012).
28. Kohn, J. E. et al. Random-coil behavior and the dimensions of chemically unfolded proteins. *Proc. Natl Acad. Sci. USA* **101**, 12491–12496 (2004).
29. Zhu, L., Wang, X., Li, J. & Wang, Y. Radius of gyration, mean span, and geometric shrinking factors of bridged polycyclic ring polymers. *Macromol. Theory Simul.* **25**, 482–496 (2016).
30. Akcora, P. et al. Anisotropic self-assembly of spherical polymer-grafted nanoparticles. *Nat. Mater.* **8**, 354–359 (2009).
31. Mitov, M., Portet, C., Bourgerette, C., Snoeck, E. & Verelst, M. Long-range structuring of nanoparticles by mimicry of a cholesteric liquid crystal. *Nat. Mater.* **1**, 229–231 (2002).
32. Gupta, M., Mohapatra, S. S., Dhara, S. & Pal, S. K. Supramolecular self-assembly of thiol functionalized pentaalkynylbenzene-decorated gold nanoparticles exhibiting a room temperature discotic nematic liquid crystal phase. *J. Mater. Chem. C* **6**, 2303–2310 (2018).
33. Dassenoy, F. et al. Platinum nanoparticles stabilized by CO and octanethiol ligands or polymers: FT-IR, NMR, HREM and WAXS studies. *N. J. Chem.* **22**, 703–712 (1998).

Acknowledgements

We thank Abdellaziz Jouaiti and Rodrigo Fernandez-Pacheco for insightful discussions, and Vanessa Soldan for assistance for cryo-TEM imaging. Financial support from Université de Toulouse (NaSAPeP grant APR), from CNRS (MITI interdisciplinary programs, COCOPIE project) and from Agence Nationale de la Recherche (PhoCatSA grant ANR-10-LABX-0037-NEXT, and MOSC grant ANR-18-CE09-0007) is acknowledged. This study has been partially supported through the EUR grant NanoX n° ANR-17-EURE-0009 in the framework of the Programme des Investissements d'Avenir.

Author contributions

S.T., C.B., G.M., H.H., M.R., and A.G. performed the experimental syntheses and characterizations; P-F.F. and A.I. performed tomography imaging by TEM; S.B. performed cryo-TEM imaging; P.R. performed SAXS measurements; J.E. performed XPS measurements; Y.C. performed HRMAS NMR measurements; S.T., C.B., and B.C. supervised the project; S.T. and C.B. conceived the project and wrote the manuscript. All authors discussed the results and commented on the manuscript.

Competing interests

The authors declare no competing interests.

Additional information

Supplementary information is available for this paper at https://doi.org/10.1038/s41467-020-15810-y.

Correspondence and requests for materials should be addressed to C.B. or S.T.

Peer review information *Nature Communications* thanks Zhihong Nie, Andreas Thünemann and the other, anonymous, reviewer(s) for their contribution to the peer review of this work. Peer reviewer reports are available.

Reprints and permission information is available at http://www.nature.com/reprints

Publisher's note Springer Nature remains neutral with regard to jurisdictional claims in published maps and institutional affiliations.

Open Access This article is licensed under a Creative Commons Attribution 4.0 International License, which permits use, sharing, adaptation, distribution and reproduction in any medium or format, as long as you give appropriate credit to the original author(s) and the source, provide a link to the Creative Commons license, and indicate if changes were made. The images or other third party material in this article are included in the article's Creative Commons license, unless indicated otherwise in a credit line to the material. If material is not included in the article's Creative Commons license and your intended use is not permitted by statutory regulation or exceeds the permitted use, you will need to obtain permission directly from the copyright holder. To view a copy of this license, visit http://creativecommons.org/licenses/by/4.0/.

© The Author(s) 2020

Supplementary information

Bidimensional lamellar assembly by coordination of peptidic polymers to platinum nanoparticles

Ghada Manai,[a,b,‡] Hend Houimel,[a,‡] Mathilde Rigoulet,[a] Angélique Gillet,[a] Pier-Francesco Fazzini,[a] Alfonso Ibarra,[c] Stéphanie Balor,[d] Pierre Roblin,[e] Jérôme Esvan,[f] Yannick Coppel,[b] Bruno Chaudret,[a] Colin Bonduelle,[b,g,*] and Simon Tricard[a,*]

[a] *Laboratoire de Physique et Chimie des Nano-Objets, INSA, CNRS, Université de Toulouse, Toulouse, France*

[b] *Laboratoire de Chimie de Coordination, CNRS, Université de Toulouse, Toulouse, France*

[c] *Instituto de Nanociencia de Aragón, Universidad de Zaragoza, Zaragoza, Spain*

[d] *Plateforme de Microscopie Électronique Intégrative, Centre de Biologie Intégrative, CNRS, Université de Toulouse, Toulouse, France*

[e] *Laboratoire de Génie Chimique, Fédération Fermat, INPT, CNRS, Université de Toulouse, Toulouse, France*

[f] *Institut Carnot – Centre Inter-universitaire de Recherche et d'Ingénierie des Matériaux, INP-ENSIACET, CNRS, Université de Toulouse, Toulouse, France*

[g] *Laboratoire de Chimie des Polymères Organiques, Université de Bordeaux, CNRS, Bordeaux INP, Pessac, France*

[*] *Corresponding authors: colin.bonduelle@enscbp.fr, tricard@insa-toulouse.fr*

[‡] *These authors contributed equally to this work*

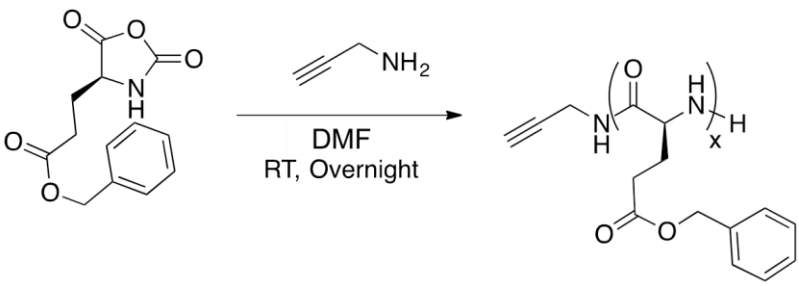

Supplementary Figure 1. PBLG synthesis. Synthetic scheme depicting poly(γ-benzyl-*L*-glutamate) (PBLG) polymers preparation. In the present study, x = 28 (**PBLG1**), 69 (**PBLG2**), 120 (**PBLG3**), 217 (**PBLG4**), 481 (**PBLG5**).

Sample	NCA	Propargyl -amine	Theoretical Dp [a]	Dp from ^{1}H NMR [b]	Mn PBLG from SEC (Dp) [c]	PDI PBLG from SEC [c]
PBLG1	2g	16 µL	30	25	6200 (28)	1.23
PBLG2	2g	8 µL	60	59	15100 (69)	1.21
PBLG3	2g	4 µL	120	92	26500 (120)	1.25
PBLG4	2g	2 µL	240	171	47500 (217)	1.25
PBLG5	2g	1.2 µL	400	373	105000 (481)	1.33

Supplementary Table 1. Chemical characterizations of the PBLG polymers. [a] Theoretical degree of polymerization ([M]/[I]); [b] Number average molar mass (Mn) determined by ^{1}H NMR (see methods). [c] Absolute number average molar mass (Mn) and dispersity (Đ) determined by SEC using a multi-angle static light scattering detection (SEC in DMF (+LiBr), see methods).

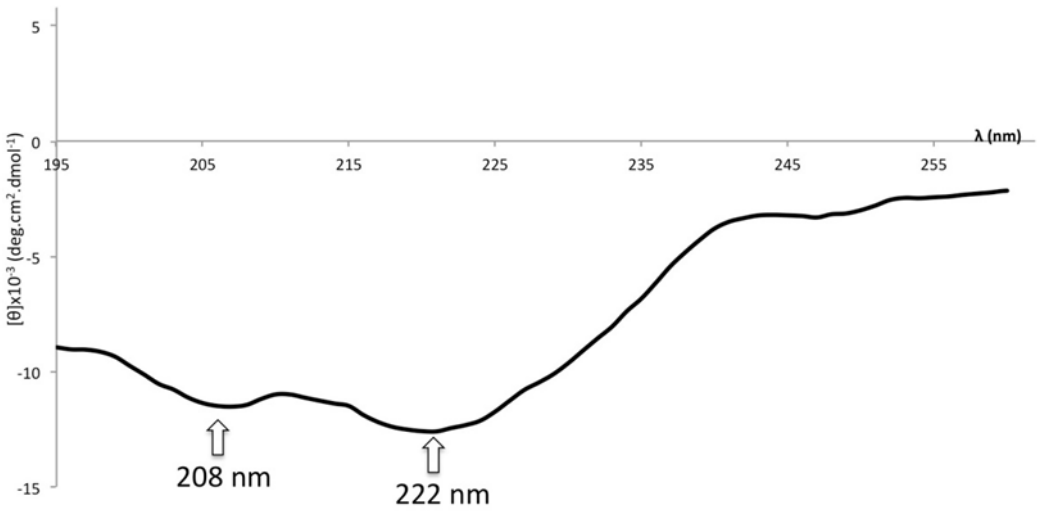

Supplementary Figure 2. Circular dichroism spectrum of PBLG4. The specific negative bands at 208 and 222 nm confirm the α-helix conformation of the polymer in THF. It is to note that the resolution of the CD measurement is strongly limited by the UV absorbance of the THF and implies the use of a specific set up before analysis (see methods).

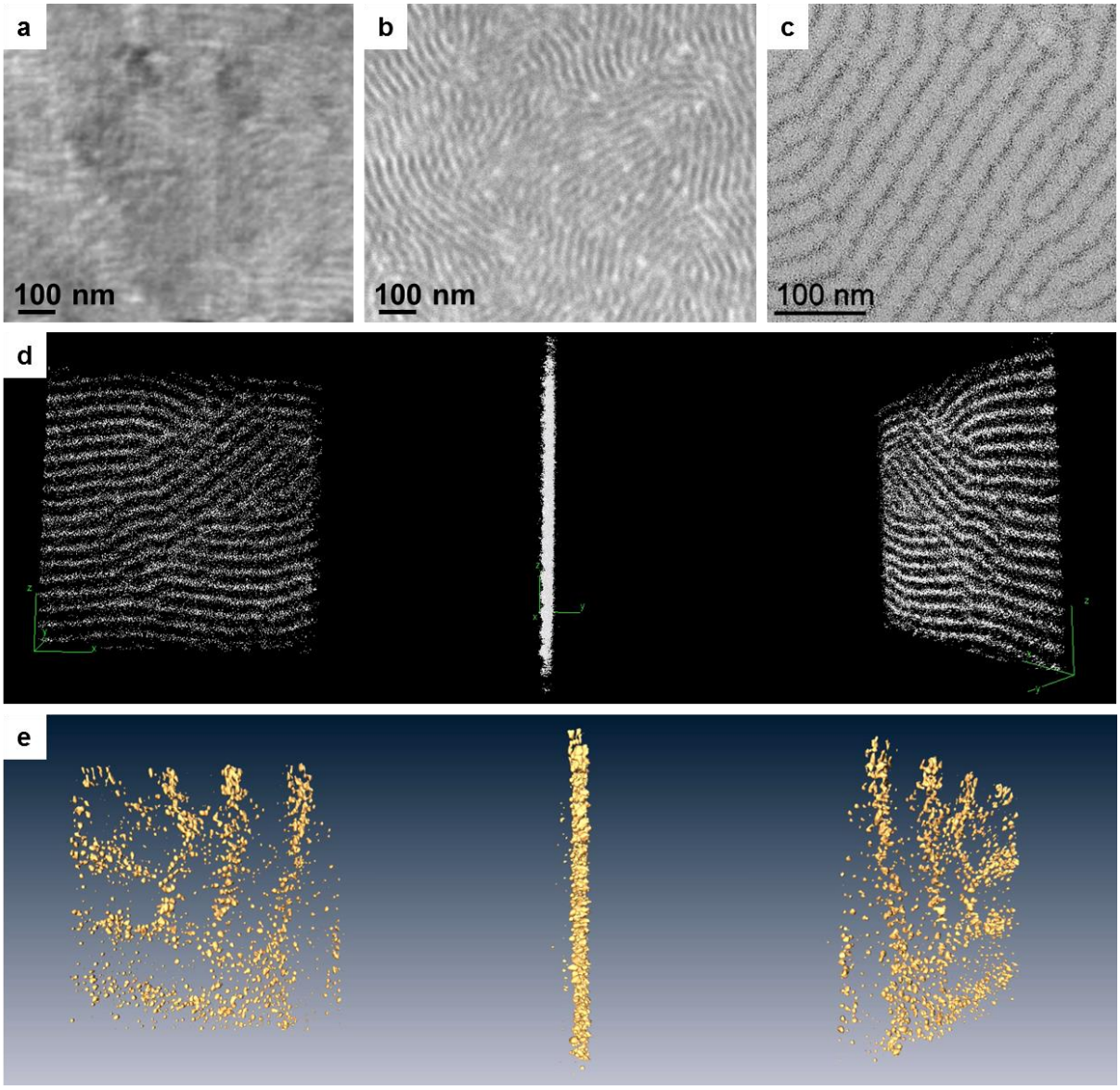

Supplementary Figure 3. Imaging of the lamellar structure of self-assembly of platinum nanoparticles with PBLG4, by different techniques: a, Atomic Force Microscopy on silicon; **b**, Scanning Electron Microscopy on silicon; **c**, Low-magnification Transmission Electron Microscopy on carbon. **d**,**e**, Tomographv 3D reconstructions at different viewing directions: **d**, at low magnification and **e**, at high magnification.

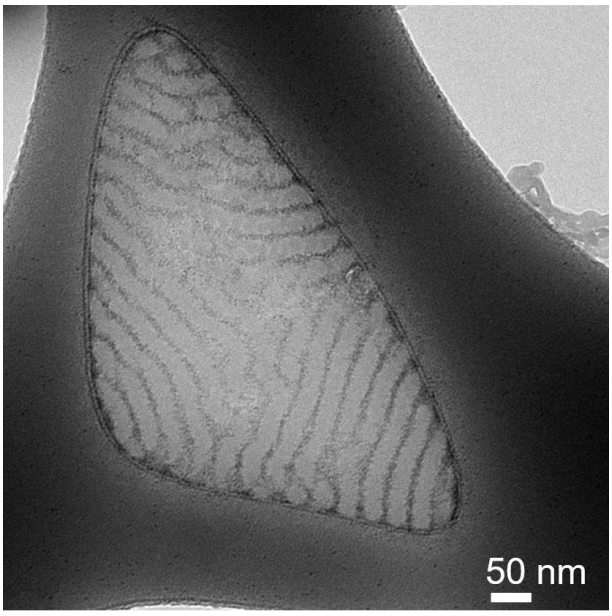

Supplementary Figure 4. Cryo-TEM imaging. Cryo-TEM imaging of self-assembly of platinum nanoparticles with **PBLG4**. Fast freezing of the THF solution confirms the presence of the lamellar structures in solution.

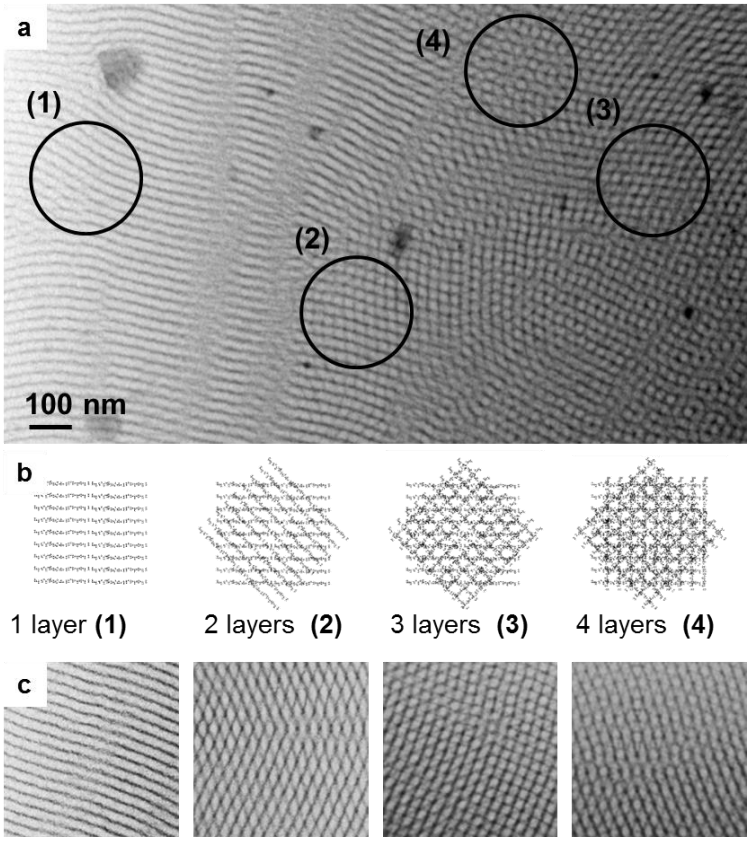

Supplementary Figure 5. Moiré patterns of lamellar self-assemblies of platinum nanoparticles with PBLG4. a, TEM image. Up to four 2D lamellar structures superimpose on each other to form specific Moiré patterns: zone (1) single layer – no Moiré, zone (2) two layers, zone (3) three layers, zone (4) four layers. **b**, Corresponding schematics for each zone, where the scheme of n layers is obtained by superimposing the scheme of 1 layer to the scheme of n-1 layers with a tilt of 45°. **c**, Picture of the same layer superimposed to itself 0, 1, 2, and 3 times after rotation; the same Moiré patterns as in zones (1) to (4) of Supplementary Fig. 5a were then artificially reconstructed.

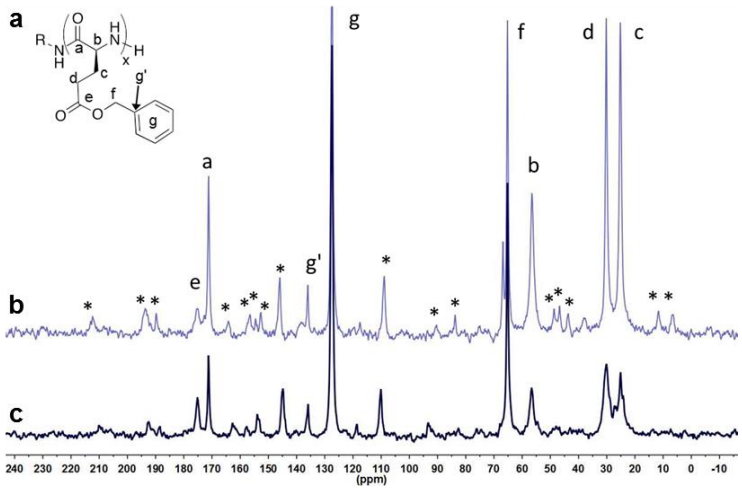

Supplementary Figure 6. ^{13}C HR-MAS NMR study of PBLG4. a, Chemical structure of PBLG, and carbon position labelling (here x = 217). **b**, Spectrum of self-assembly of platinum nanoparticles with **PBLG4**. **c**, Spectrum of **PBLG4** alone. The spectra were obtained in THF at 1,8 kHz (* = rotation bands). The appearance of new rotation bands and the narrowing of the polymer peaks show a rigidifying of the polymer structures in the self-assembly.

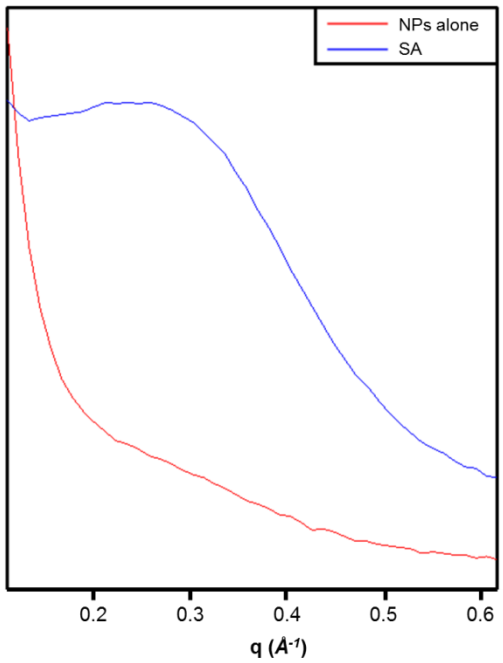

Supplementary Figure 7. Interparticle distance. Small angle X-ray scattering patterns for platinum nanoparticles alone (without PBLG – NPs alone) and for the self-assembly of platinum nanoparticles with **PBLG4** (SA). The nanoparticles alone don't show any specific signal in addition to the continuous background, whereas the self-assembly shows a broad peak, which corresponds to a specific correlation distance between the nanoparticles equal to 2.5 nm ($2\pi / q_{max}$).

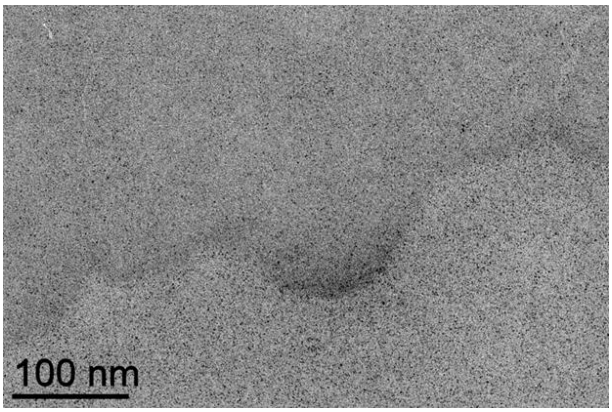

Supplementary Figure 8. Absence of self-assembly in high quantity of PBLG. TEM micrograph of mixing of platinum nanoparticles with 5eq. of **PBLG4**.

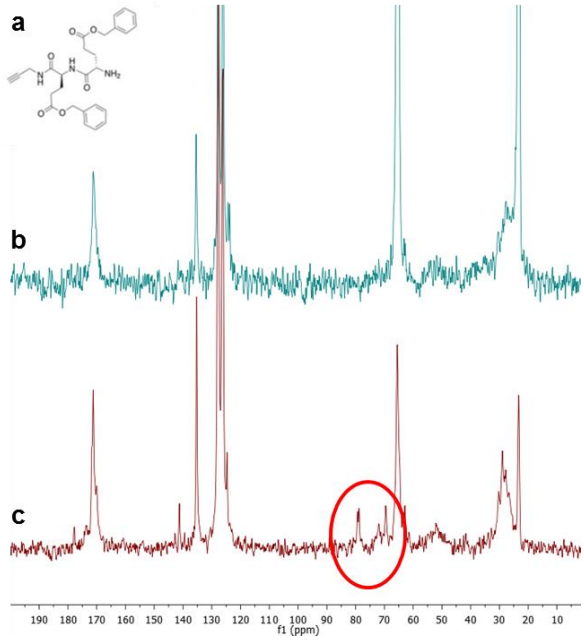

Supplementary Figure 9. ^{13}C solid-state MAS NMR study of DBLG. a, Chemical structure of **DBLG**. **b**, Spectrum of self-assembly of platinum nanoparticles with **DBLG**. **c**, Spectrum of **DBLG** alone. The spectra were obtained at 10 kHz. The disappearing of the peaks at 72 and 80 ppm is in agreement with the coordination of the alkyne moiety of the polymer to the nanoparticle surface in the self-assembly.

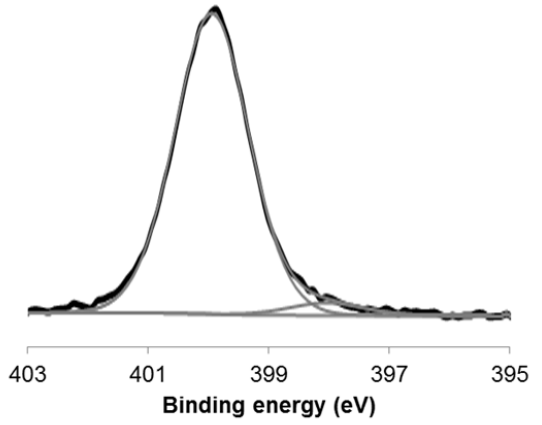

Supplementary Figure 10. Reduced component at 5 eq. XPS spectrum at the N*1s* edge of mixing of platinum nanoparticles with 5eq. of **PBLG4** (4% of contribution at 398 eV). We start to observe the appearance of the reduced contribution of nitrogen at 5 eq.

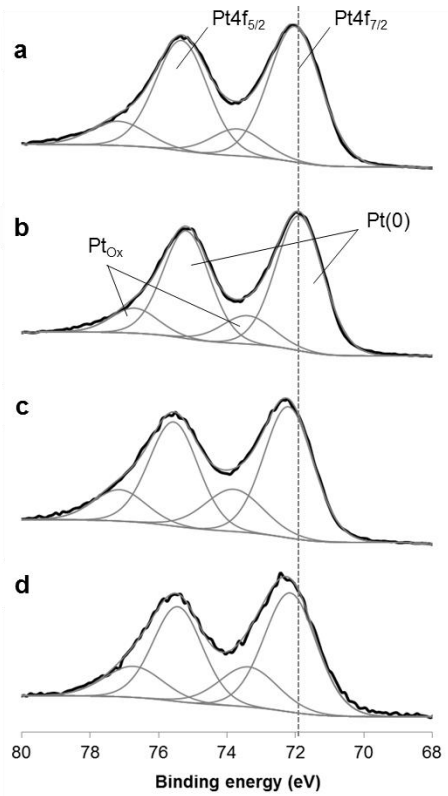

Supplementary Figure 11. Relative oxidation of platinum upon addition of PBLG. XPS spectra at the Pt*4f* edge of assemblies between platinum nanoparticles and **PBLG4** at: a, 0.05 eq. (18% of oxidized contribution); b, 0.5 eq. (19% of oxidized contribution); c, 1 eq. (26% of oxidized contribution); d, 5 eq. (28% of oxidized contribution). The progressive increase of the oxidized contribution at ~73.4 and ~76.7 eV from 0.05 eq. to 5 eq. and the slight increase of the global Pt*4f* binding energies (a dashed line is added as a guide for the eye) confirmed an increase of the relative platinum oxidation at the NP surface upon addition of PBLG.

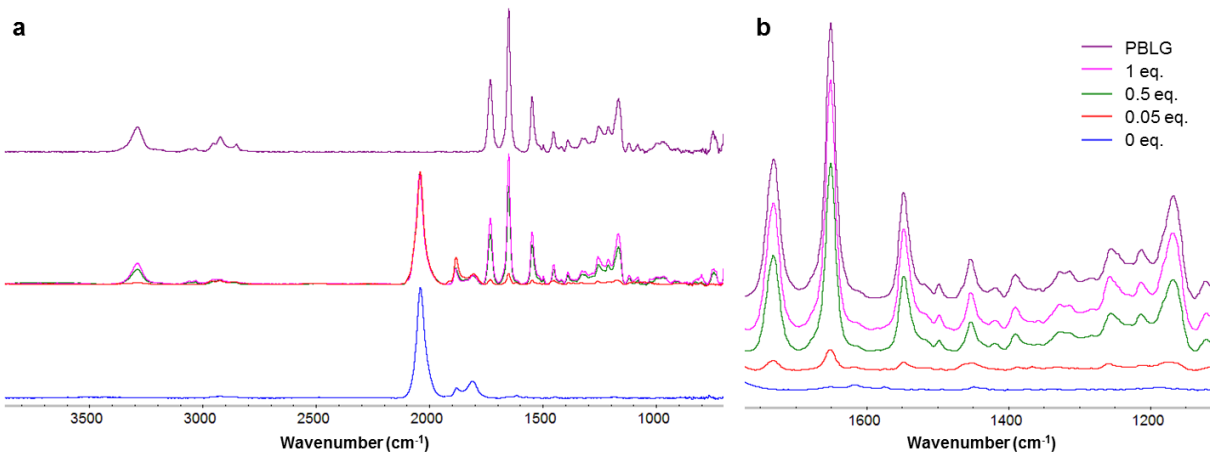

Supplementary Figure 12. FT-IR spectra. a, Full range FT-IR spectra of **PBLG4** alone and of the self-assemblies between platinum nanoparticles and **PBLG4** (at 0 eq., 0.05 eq., 0.5 eq., and 1 eq.) and **b**, zoom on the **PBLG4** fingerprint region – the spectra are shifted for clarity. The esters (1770 cm^{-1}) and amide (1770 cm^{-1} and 1770 cm^{-1}) vibrations are not affected by the NP addition. The spectra are normalized on the signal of the CO vibration around 2040 cm^{-1}.

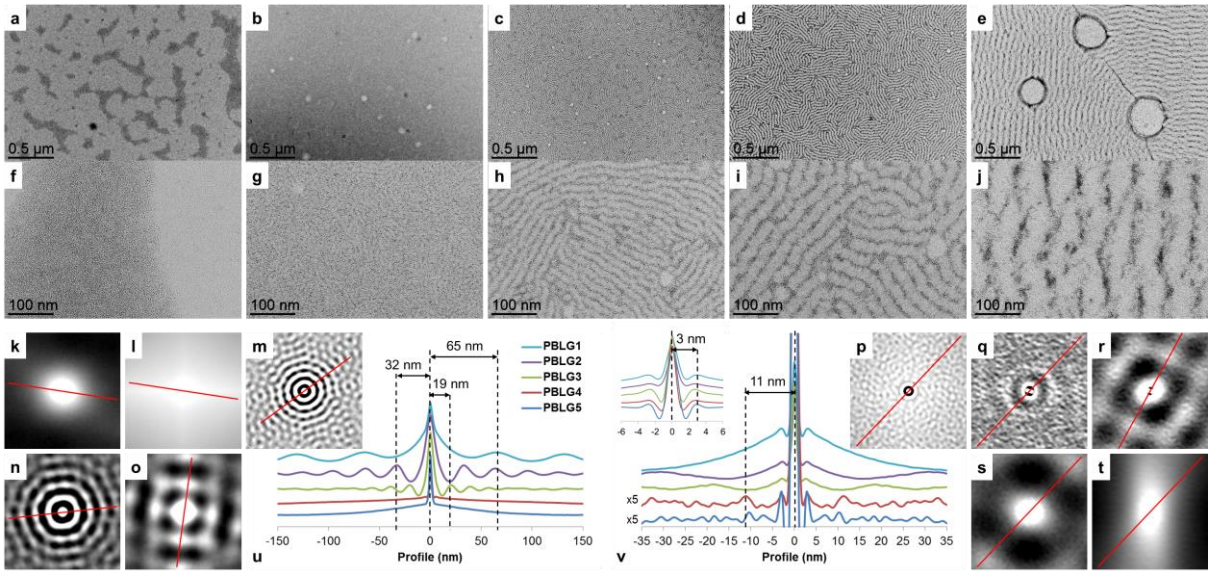

Supplementary Figure 13. Effect of the degree of polymerization – image analysis. TEM micrographs at two scales of self-assemblies between platinum nanoparticles and: **a**, **f**, **PBLG1**; **b**, **g**, **PBLG2**; **c**, **h**, **PBLG3**; **d**, **i**, **PBLG4**; and **e**, **j**, **PBLG5**. Autocorrelation images of : **k**, a; **l**, b; **m** c; **n**, d; **o**, e; **p**, f; **q**, g; **r**, h; **s**, i; **t**, j. **u**, Profiles represented on images k, l, m, n, and o. **v**, Profiles represented on images p, q, r, s, and t. (Inset : zoom on the central region of the profile). Systematic image analysis gives the average periodicity of the lamellas as shown on Fig. 4f and Supplementary Table 2.

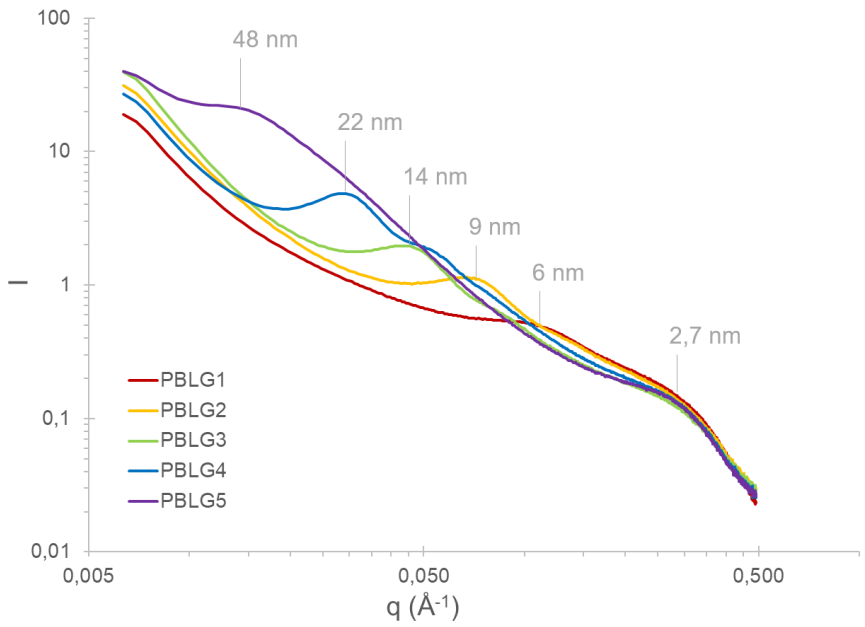

Supplementary Figure 14. SAXS measurements. SAXS measurements on self-assemblies between platinum nanoparticles and **PBLG1**, **PBLG2**, **PBLG3**, **PBLG4**, and **PBLG5**. The SAXS curves show the presence of multiple correlation peaks. For all samples, the large peak around 0.23 $Å^{-1}$ gives an average distance of 2.7 nm corresponding to the correlation distance between the nanoparticles, as already observed (Supplementary Fig. 7). The presence of one peak (for **PBLG1** and **PBLG2)** or two peaks (for **PBLG2**, **PBLG3** and **PBLG4**) in the first part of the curve comes from interactions at medium distances, and proves the presence of the lamellae in the macroscopic sample. The corresponding periodicities deduced from the position of the first peak are represented on the curves and reported in Supplementary Table 2. The second peak, when distinguishable, corresponds to the harmonic at a double *q* value, confirming the spacing is constant at higher distances than a single period. The SAXS measurements confirmed the increasing of the average inter-lamellar distance with the degree of polymerization. The broadness of the peaks reflects a distribution of distances, as observed by TEM imaging.

Periodicity (nm)	TEM	SAXS
PBLG1	-	6
PBLG2	11	9
PBLG3	19	14
PBLG4	32	22
PBLG5	65	48

Supplementary Table 2. Comparison of the periodicities of the self-assemblies obtained by TEM (Supplementary Fig. 13) and SAXS (Supplementary Fig. 14) measurements. Structural and microscopy analyses gave coherent trends, where the periodicity of the lamellae increased with the degree of polymerization of the polymer. Differences of absolute values can be explained by the beginning of precipitation occurring during the SAXS measurements (and thus to a compression of the system due to the solvent exclusion). On the contrary, sample preparation for electron microscopy corresponds to a quenching of the system in solution (as the solvent is rapidly absorbed by a filter paper during the TEM grid preparation). The periodicity for the cryo-TEM images with **PBLG4** was found to be 31 nm (Supplementary Fig. 4), in line with the TEM measurements.

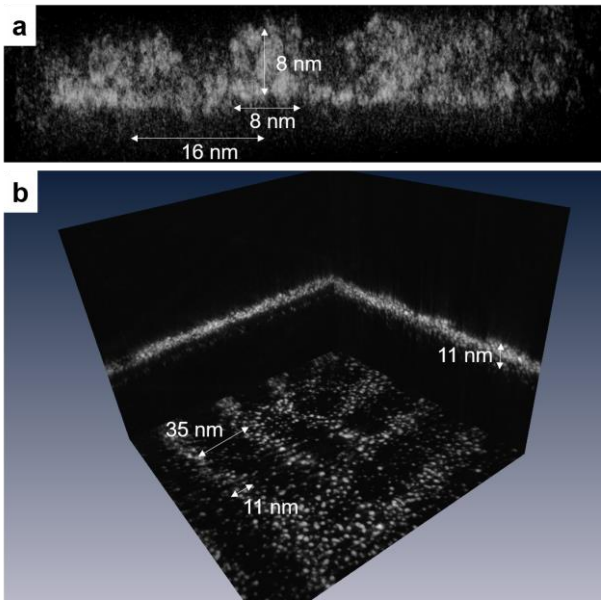

Supplementary Figure 15. Geometrical analysis of tomography reconstructions. Analysis of tomography reconstruction of self-assemblies between platinum nanoparticles and: **a**, **PBLG3** and **b**, **PBLG4** confirmed similar thicknesses and width of the NP containing zones. The local periodicity is coherent with average values obtained by systematic image analysis (Fig. 4, Supplementary Fig. 13, and Supplementary Table 2).

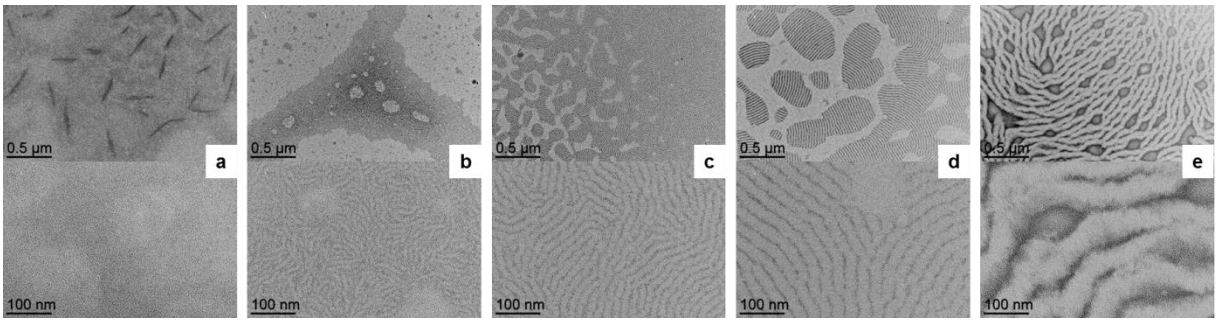

Supplementary Figure 16. Effect of the degree of polymerization. TEM micrographs at two scales of self-assemblies, keeping the polymer on nanoparticle ratio constant between platinum nanoparticles and **a**, **PBLG1** (0.06 eq.). **b**, **PBLG2** (0.16 eq.). **c**, **PBLG3** (0.28 eq.). **d**, **PBLG4** (0.50 eq.). **e**, **PBLG5** (0.81 eq.). Similar structures are obtained by keeping the monomer units per nanoparticle (Supplementary Fig. 13a to j) or the polymer number per nanoparticle constant.

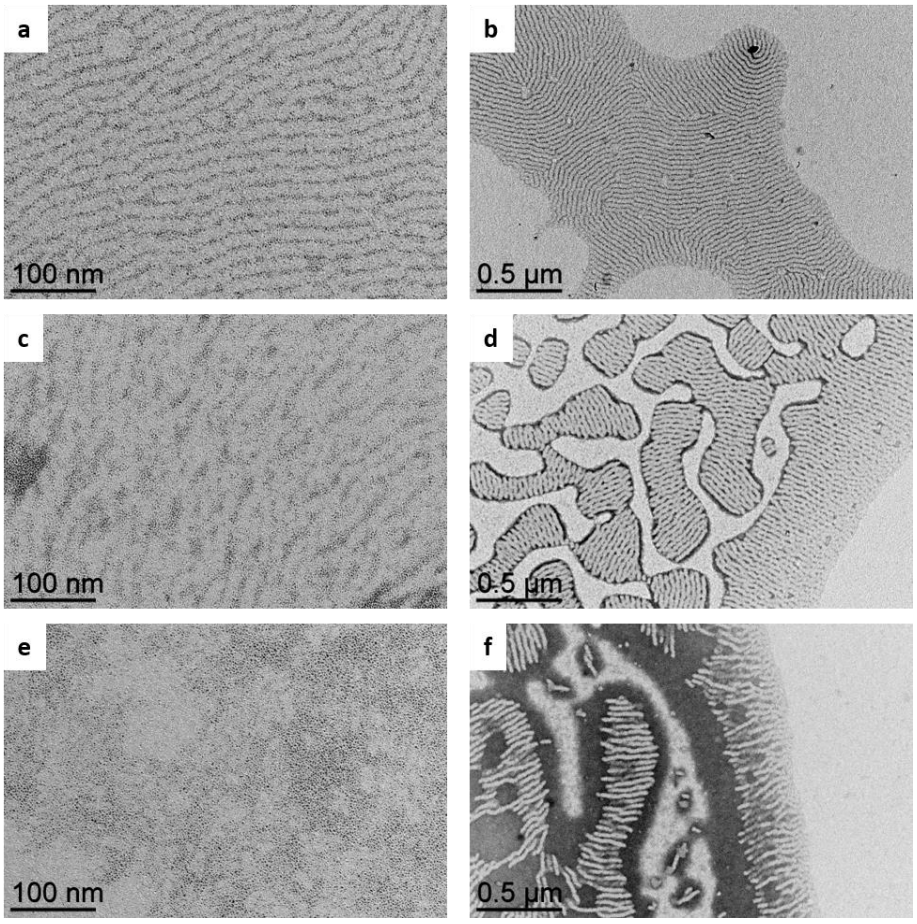

Supplementary Figure 17. First steps of self-assembly. TEM micrographs of self-assemblies between platinum nanoparticles and **a**, **c**, **e**: **PBLG3**; **b**, **d**, **f**: **PBLG4**: **a**, **b**: after 2 h of reaction. **c, d**: after 5 s of reaction. **e, f**: after a fraction of second of reaction – the nanoparticles are drop-casted on pre-deposited PBLG. The assembly behavior was comparable at the two different Dp (see main text).

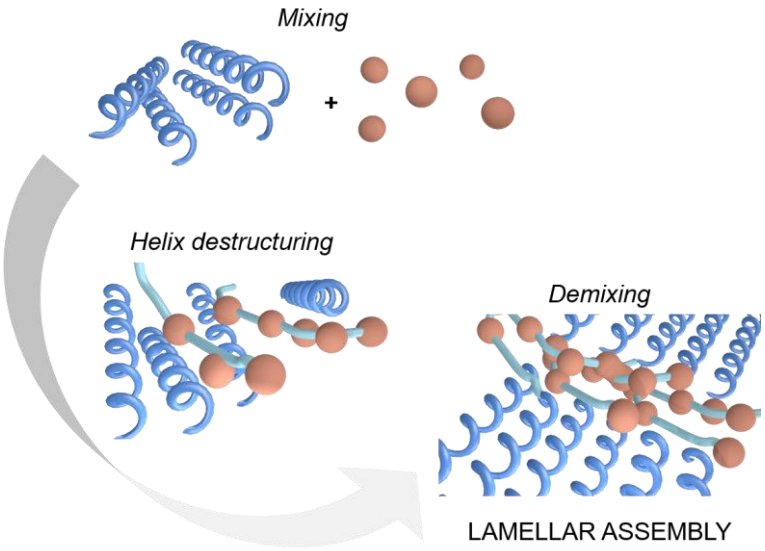

Supplementary Figure 18. Scheme of the self-assembly process. α-helices of PBLG tend to spontaneously align in THF solution. Upon mixing with platinum nanoparticles, some part of them are destructured thanks to interaction with their amide functional groups and the nanoparticle surface, and form random coils that interact with an average of 6-7 nanoparticles. Demixing between such a hybrid phase and the excess of PBLG in α-helices led to the alternation of lamellae, stabilized by the coordination of the alkyne terminal group of the polymer to the surface of accessible nanoparticles.

Reviewers' comments:

Reviewer #1 (Remarks to the Author):

The authors produced mixtures of nanoparticles and a homopolymer in THF as solvent. The nanoparticles were very spherical Pt nanoparticles with a diameter of 1.2 ± 0.3 nm as determined with electron microscopy. The homopolymer was poly(gamma-benzyl-L-glutamate) with different molar masses. In The absence of nanoparticles this polymer forms an alpha helix in THF.
The new finding of the work is that lamellar nanostructures are formed upon mixing. This lamellar phase consists of alternating lamellae of type 1 and type 2. The lamellae of type 1 are enriched in nanoparticles while no nanoparticles are present in type 2. This was visualized with TEM and found for a wide range of compositions.
Similar nanostructures are well reported for block-copolymers but not for homopolymers. The explanation for such nanoparticle-enriched lamellae in block-copolymers is straight-forward as can be found in the literature cited by the authors.
Normally one expects that either the polymer decorates the nanoparticle or vice versa the nanoparticles decorate the polymer. Such depend to the molar masses, concentrations, strength of interaction of the polymers and the nanoparticles etc.
But the formation of lamellar structures of the named homopolymer is highly unexpected and to me not sufficiently explained by the authors. For each polymer chain the nanoparticles need to induce a change of the conformation from an alpha helix to a random coil. But only for that fraction of the chain which is then located in the nanoparticle-rich lamellae type 1. The remaining part of each chain is still in an alpha-helical conformation forming lamellae type 2. When assuming this mechanism, a kind of pseudo block-copolymer is formed: therein block 1 is the random coil and block 2 is the alpha helix. In principle such is possible and can explain the lamellar structures. But such scenario is very unlikely.
Instead, I assume that the lamellar structures are formed during deposition of the mixtures on surfaces prior to TEM measurements. It needs to be excluded that a phenomenon similarly to the coffee ring effect produces the lamellar structures. Further experiments for ensemble averaging data are needed.
The authors are already going in the right direction with their SAXS measurements. But the SAXS data presented in Figure S6 is absolutely not sufficient. The peak in the scattering curve could simply result from a so-called correlation hole as found for many polymeric structures. The peak is no proper evidence for the existence of a lamellar structure in solution. Here a reasonable modelling of the SAXS curves is needed and data should be measured from all the samples that correspond to the TEM pictures presented in Figures 1 and 2. The SAXS measurements should be performed from samples in solution in a capillary. Otherwise the data are prone to artifacts. A normal lab SAXS instruments is suitable. The lamellar structures must provide a very strong scattering intensity and a distinctive scattering pattern, if they exist in solution as claimed by the authors. Data evaluation can be performed with open source small-angle scattering programs. These programs provide appropriate models for lamellar structures to simulate the measured curves.
In summary, the manuscript needs major revision that provides clear evidence for the presence of the lamellar structure in solution.

Reviewer #2 (Remarks to the Author):

The entitled work “Beyond Flory-Huggins theory: bidimensional lamellar assembly by coordination of peptidic homopolymers to platinum nanoparticles” by Manai et al. reported the use of homopolymers to control the organization of nanoparticles. The authors confirmed that PBLG polypeptide homopolymers coordinated with nanoparticles by 13C NMR spectroscopy. We could imagine that the homopolymers formed brush layers on the surfaces of nanoparticles, which makes this system perfectly fit into the frame of the Flory-Huggins theory. In previous studies, the

phase behaviors of the conjugates (or amphiphiles) of nanoparticles, e.g. Au NPs (Mei et al. Chem Eur J 2019, 1) or POSS (Wu et al. Macromolecules 2014, 4622; Zhang et al. Soft Matter 2019, 7108), and polymers have been well documented. The PBLG-Pt nanoparticle conjugates in this work were in-situ generated upon the mixing of PBLG and Pt nanoparticles, which made it different from previous reports on ex-situ synthesized nanoparticle-polymer conjugates. This work does not have enough novelty for publication in Nature Communications.

Additional comments:
1. The authors claimed that the lamellar structures formed in the solution, but they characterized the films after the evaporation of solvent. It would be more convincing to use cryo-TEM to characterize the solution structure.

2. The exact structure is still unclear. It will be helpful to capture the structures at the early stage and characterize the kinetics of the self-assembly process.

3. The use of "Beyond the Flory-Huggins theory" in the tile might not be appropriate.

Reviewer #3 (Remarks to the Author):

The manuscript by Manai et al. describes the self-assembly of a mixture of small platinum nanoparticles (NP) and poly(benzyl-L-glutamate) (PBLG) into periodic lamellar structures. The formation of microphase-separated structures is driven by the coordination interactions between the surface of NPs and the functional groups of PBLG. The authors systematically investigated the effect of substrates, polymer length, and volume ratio of NPs to polymers on the assembly morphologies. The present work expands on the mechanism of polymer-guided assembly of inorganic NPs in films.

The presented work is sound, and experimental data gives deep insight into the assembly of polymer-NP composites. There is no doubt that this paper reports significant advancement in a field. Thus, I would recommend the publication of this work in Nature Communications, after few concerns are addressed:

1. The authors carefully characterized the interactions between NPs and PBLG. However, it is still not straightforward for readers to understand how the lamellar structures are formed on the basis of these interactions. I would suggest the authors include a new scheme illustrating the mechanism of microphase separation in the main text or SI.

2. Is it possible that the immiscibility between the exposed surface of NPs and homopolymers is the driving force of phase separation? One quick experiment may be considered to verify this possibility: mixing and assembling NPs with homopolymers (e.g., PS) with the same end functional group.

3. What is the thickness of the films? Is the assembly morphology dependent on the film thickness?

4. The formation of Moiré patterns in the assembly is interesting and rarely observed in polymer systems. Why? A reasonable explanation would be very helpful.

5. Some figure captions are not clear:
a. "Figure 1 Building blocks...", but this figure includes both building blocks and assembly structures.
b. "...Evolution of characteristic widths as a function of the degree of polymerization x: squares:

average periodicity of the lamellas; white circles: average width of the white...". The format is a bit confusing.

Response to the reviewers.

Reviewers' comments:

Reviewer #1 (Remarks to the Author):

The authors produced mixtures of nanoparticles and a homopolymer in THF as solvent. The nanoparticles were very spherical Pt nanoparticles with a diameter of 1.2 ± 0.3 nm as determined with electron microscopy. The homopolymer was poly(gamma-benzyl-L-glutamate) with different molar masses. In The absence of nanoparticles this polymer forms an alpha helix in THF.
The new finding of the work is that lamellar nanostructures are formed upon mixing. This lamellar phase consists of alternating lamellae of type 1 and type 2. The lamellae of type 1 are enriched in nanoparticles while no nanoparticles are present in type 2. This was visualized with TEM and found for a wide range of compositions.
Similar nanostructures are well reported for block-copolymers but not for homopolymers. The explanation for such nanoparticle-enriched lamellae in block-copolymers is straight-forward as can be found in the literature cited by the authors.
Normally one expects that either the polymer decorates the nanoparticle or vice versa the nanoparticles decorate the polymer. Such depend to the molar masses, concentrations, strength of interaction of the polymers and the nanoparticles etc.
But the formation of lamellar structures of the named homopolymer is highly unexpected and to me not sufficiently explained by the authors.

Following the remarks of Reviewer #1, and suggestions of Reviewer #2 and Reviewer #3, several additions has been made in the manuscript in order to explain better the formation of the lamellar structure.

A paragraph has been added to describe the self-assemblies at short times of mixing (p. 7), the Discussion section is now more detailed (p. 7-8) and an explicative figure has been added in SI (Fig. S18).

For each polymer chain the nanoparticles need to induce a change of the conformation from an alpha helix to a random coil. But only for that fraction of the chain which is then located in the nanoparticle-rich lamellae type 1. The remaining part of each chain is still in an alpha-helical conformation forming lamellae type 2. When assuming this mechanism, a kind of pseudo block-copolymer is formed: therein block 1 is the random coil and block 2 is the alpha helix. In principle such is possible and can explain the lamellar structures. But such scenario is very unlikely. Instead, I assume that the lamellar structures are formed during deposition of the mixtures on surfaces prior to TEM measurements. It needs to be excluded that a phenomenon similarly to the coffee ring effect produces the lamellar structures. Further experiments for ensemble averaging data are needed.

The coffee ring effect is a pattern left by a puddle of particle-laden liquid after it evaporates. It originates from combination of evaporation of solvent, capillary flow and Marangoni flow. It has a purely physical origin. Such an effect has been observed in our systems, and influenced the morphology of the assemblies at the micrometer scale, as shown in the picture below.

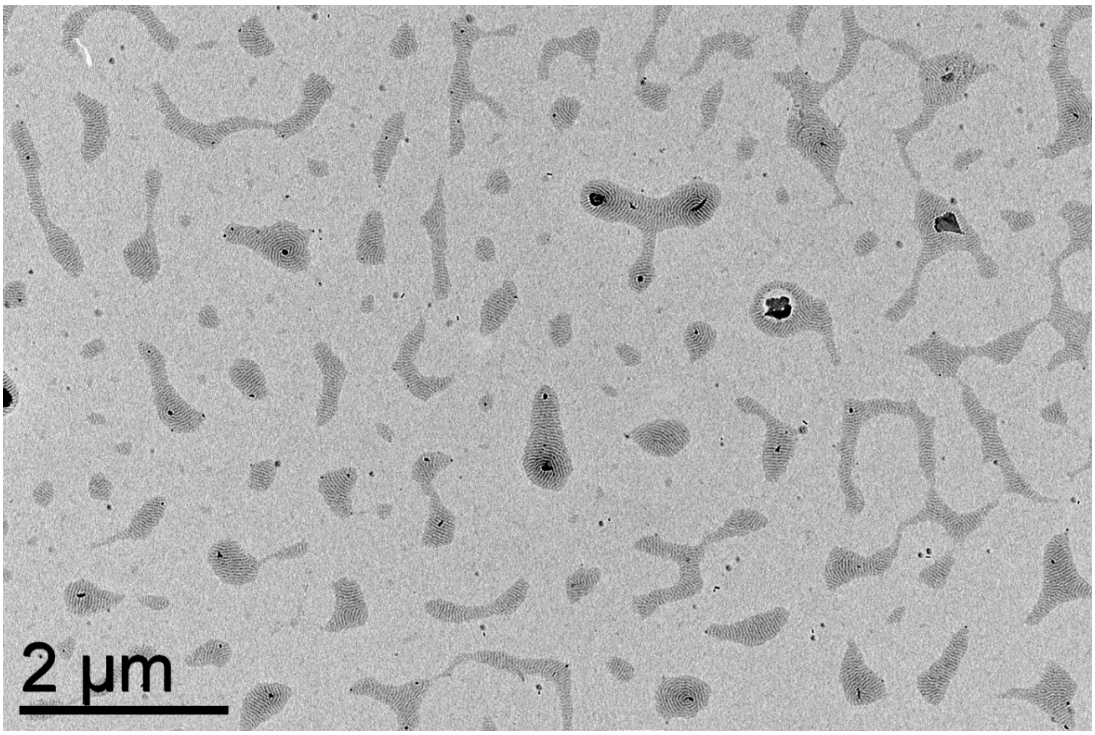

We prefer avoiding speaking about coffee ring effect in the present manuscript, as it is in the margin of the main message: a description of the superstructures at the nanometer scale, where the main driving forces of the assembly are dipolar interactions and molecular interaction, such as Van der Waals forces or coordination bounds.

The authors are already going in the right direction with their SAXS measurements. But the SAXS data presented in Figure S6 is absolutely not sufficient. The peak in the scattering curve could simply result from a so-called correlation hole as found for many polymeric structures. The peak is no proper evidence for the existence of a lamellar structure in solution. Here a reasonable modelling of the SAXS curves is needed and data should be measured from all the samples that correspond to the TEM pictures presented in Figures 1 and 2. The SAXS measurements should be performed from samples in solution in a capillary. Otherwise the data are prone to artifacts. A normal lab SAXS instruments is suitable. The lamellar structures must provide a very strong scattering intensity and a distinctive scattering pattern, if they exist in solution as claimed by the authors. Data evaluation can be performed with open source small-angle scattering programs. These programs provide appropriate models for lamellar structures to simulate the measured curves.

As asked by Reviewer #1, SAXS measurements have been performed on assemblies with **PBLG1** to **PBLG5**. In addition to confirming a constant inter-particle average distance, such measurements proved the coherence of the lamellar structure at the macroscopic scale and confirmed an increase of the inter-lamellar distance with the degree of polymerization of the PBLG.

The corresponding figure and a table comparing the periodicities in TEM and SAXS have been added in SI (Fig. S14 and Table S2). A new sentence has been added in the main manuscript (p. 6), and the experimental section has been completed accordingly (p. 11). Pierre Roblin, who conceived and performed the SAXS measurements, has been added to the list of co-authors.

In summary, the manuscript needs major revision that provides clear evidence for the presence of the lamellar structure in solution.

To get signals in SAXS, we had to concentrate the samples and measurements were performed at the beginning of precipitation. To provide clear evidence of the presence of the lamellar structure in solution, we also performed cryo-TEM microscopy (as suggested by Reviewer #2). After adaptation of the classical cryo-TEM techniques to work with THF, we succeeded in observing the lamellae in solution.

This supplementary characterization provides a direct and indisputable proof of the presence of lamellae in solution. A corresponding figure has been added in SI (Fig. S4) and a descriptive sentence has been added in the main text (p. 4). Stéphanie Balor, who conceived and performed the cryo-TEM imaging, has been added to the list of co-authors.

Reviewer #2 (Remarks to the Author):

The entitled work “Beyond Flory-Huggins theory: bidimensional lamellar assembly by coordination of peptidic homopolymers to platinum nanoparticles” by Manai et al. reported the use of homopolymers to control the organization of nanoparticles. The authors confirmed that PBLG polypeptide homopolymers coordinated with nanoparticles by 13C NMR spectroscopy. We could imagine that the homopolymers formed brush layers on the surfaces of nanoparticles, which makes this system perfectly fit into the frame of the Flory-Huggins theory. In previous studies, the phase behaviors of the conjugates (or amphiphiles) of nanoparticles, e.g. Au NPs (Mei et al. Chem Eur J 2019, 1) or POSS (Wu et al. Macromolecules 2014, 4622; Zhang et al. Soft Matter 2019, 7108), and polymers have been well documented. The PBLG-Pt nanoparticle conjugates in this work were in-situ generated upon the mixing of PBLG and Pt nanoparticles, which made it different from previous reports on ex-situ synthesized nanoparticle-polymer conjugates. This work does not have enough novelty for publication in Nature Communications.

Whereas the references proposed by Reviewer #2 are very interesting, the mechanism proposed therein cannot describe the system presented in our manuscript. First, we observed coordination of the peptide bonds of the polymers to the nanoparticles surface. This experimental observation clearly rules out the formation of simple conjugates composed of two "blocks", *i.e.* in our case, nanoparticles only linked by the end-alkyne terminal groups of the polymer. Second, in the references mentioned by Reviewer #2, the rod behavior of the system is provided by the inorganic part of the conjugate; we then agree that the behavior of the organic part is in agreement with the Flory-Huggins theory. In marked contrast, it is the organic part – the PBLG part adopting α-helical conformation – that exhibits the rod-like behavior in our system. Based on the data from Figure 4 and Table S2, we can establish a scaling law of the lamellae thickness *vs.* the average molar mass proportional to $Mn^{0.98}$ (see the figure below). With diblock copolymers, a bibliographic study indicates that a scaling law exponent of lamellae thickness vs. molar mass varies experimentally from 0.5 for the lower masses (*e.g.* < 10000 g/mol) to 0.7 for the larger ones (Sandre Olivier et al., Polymer, 2010, 21 (21), 4673-4685). These values are in principle close to the reference exponent of 0.643 predicted by Helfand (Helfand, E., Macromolecules 1975,8, 552-556; Helfand, E.; Wasserman, Z. R., Macromolecules 1976,9, 879-888), which is significantly lower than the exponent value of 0.98 estimated from our data.

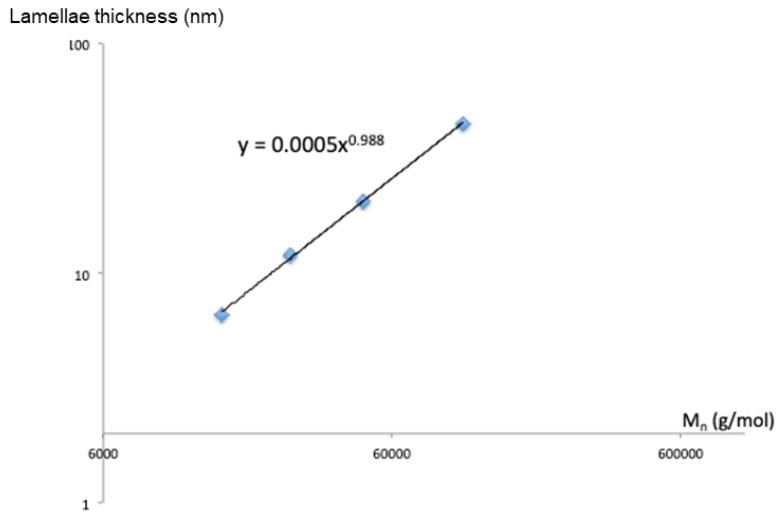

Additional comments:

1. The authors claimed that the lamellar structures formed in the solution, but they characterized the films after the evaporation of solvent. It would be more convincing to use cryo-TEM to characterize the solution structure.

The experiment has been done and gave convincing results. We thank Reviewer #2 for his suggestion.

A corresponding figure has been added in SI (Fig. S4) and a descriptive sentence has been added in the main text (p. 4).

2. The exact structure is still unclear. It will be helpful to capture the structures at the early stage and characterize the kinetics of the self-assembly process.

Regular experiments are done with 2 hours of agitation to be sure to reach a steady state. Following Reviewer #2's suggestion, we explored very short time of reactions and noticed the structures are generally formed after 5 min. Specific experiments have thus been done to catch the very beginning of the self-assembly process, which turns out to start in the first seconds of mixing.

To take into account this comment, a descriptive paragraph has been added in the main text (p. 7), and a corresponding figure has been added in SI (Fig. S17).

3. The use of "Beyond the Flory-Huggins theory" in the tile might not be appropriate.

Even if we are convinced that our systems cannot be described by the conventional formalism developed for diblock-copolymer, as detailed above, we decided to modify the title in line with Reviewer #2's comment.

Reviewer #3 (Remarks to the Author):

The manuscript by Manai et al. describes the self-assembly of a mixture of small platinum nanoparticles (NP) and poly(benzyl-L-glutamate) (PBLG) into periodic lamellar structures. The formation of microphase-separated structures is driven by the coordination interactions between the surface of NPs and the functional groups of PBLG. The authors systematically investigated the effect of substrates, polymer length, and volume ratio of NPs to polymers on the assembly morphologies. The present work expands on the mechanism of polymer-guided assembly of inorganic NPs in films.

The presented work is sound, and experimental data gives deep insight into the assembly of polymer-NP composites. There is no doubt that this paper reports significant advancement in a field. Thus, I would recommend the publication of this work in Nature Communications, after few concerns are addressed:

1. The authors carefully characterized the interactions between NPs and PBLG. However, it is still not straightforward for readers to understand how the lamellar structures are formed on the basis of these interactions. I would suggest the authors include a new scheme illustrating the mechanism of microphase separation in the main text or SI.

A corresponding figure has been added in SI (Fig. S18) and the Discussion section of the main text is now more detailed (p. 7-8).

2. Is it possible that the immiscibility between the exposed surface of NPs and homopolymers is the driving force of phase separation? One quick experiment may be considered to verify this possibility: mixing and assembling NPs with homopolymers (e.g., PS) with the same end functional group.

The experiment has been done using PS with a DP of 336, in the same order of magnitude as the one used for PBLG in exactly the same experimental conditions. We see in TEM imaging (see picture below - left) that some kind of structuration appears, but clearly different from the well-ordered lamellae obtained with PBLG. Immiscibility between the homopolymer and the NP zone thus clearly plays a role in the structuration, but the presence of coordinating groups is crucial to go a step further and interact with the NP, as detailed throughout the manuscript. If the system is only governed by repulsive forces, arrangement between the components generally tends to form isotropic structure (like the spherical aggregates observed with PS – see picture below - right). There might be some interest to study such a phenomenon in more details in the scope of a separate study.

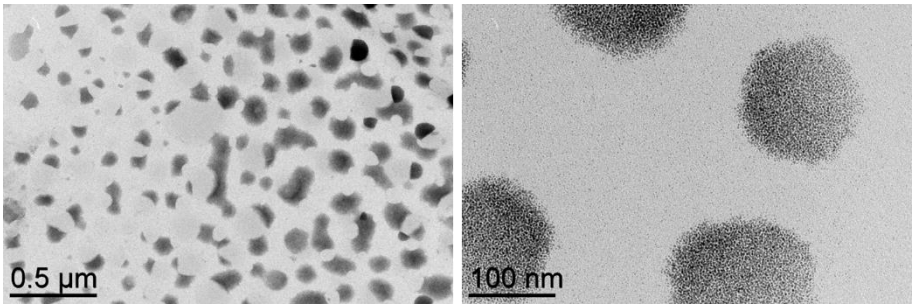

3. What is the thickness of the films? Is the assembly morphology dependent on the film thickness?

Analysis of the tomography picture already obtained for **PBLG4** showed that the thickness of the film is comparable to the width of the NP lamella. We performed tomography microscopy with **PBLG3** to confirm this trend.

A corresponding figure has been added in SI (Fig. S15) and a descriptive sentence has been added in the main text (p. 6).

4. The formation of Moiré patterns in the assembly is interesting and rarely observed in polymer systems. Why? A reasonable explanation would be very helpful.

Thanks to the present revision of the manuscript, we have demonstrated that the assembly formed in solution. If the lamellae are pre-formed in solution, they can deposit on top of each other during the drop casting of the TEM grid preparation, if the solution is sufficiently concentrated. We should notice that such an effect has been observed by chance. It will be of interest to study it in more details the scope of another work. But we think it is interesting to mention it in the present manuscript as it gives a supplementary indirect proof of the existence of the lamellae in solution.

A sentence of explanation as been added in the main text (p. 4).

5. Some figure captions are not clear:
a. "Figure 1 Building blocks...", but this figure includes both building blocks and assembly structures.

The caption has been corrected (p. 16).

b. "...Evolution of characteristic widths as a function of the degree of polymerization x: squares: average periodicity of the lamellas; white circles: average width of the white...". The format is a bit confusing.

A legend has been added in the figure and the caption has been adapted (p.19).

REVIEWERS' COMMENTS:

Reviewer #2 (Remarks to the Author):

I agreed with the argument in the response "This experimental observation clearly rules out the formation of simple conjugates composed of two "blocks", i.e. in our case, nanoparticles only linked by the end-alkyne terminal groups of the polymer. " It did not form a 'diblock" conjugate, but they are hairy nanoparticles with PLBG as the corona. The difference is that PLBG had rod-like conformation, while the polymers in previous studies might form random coils. I suggested the authors acknowledging previous works on nanoparticle-polymer conjugates in the revised version.

Reviewer #3 (Remarks to the Author):

The authors have performed additional experiments and addressed the comments raised by the reviewers. The revised manuscript is now suitable for publication in Nature Communications as is.

Response to the reviewers.

Reviewers' comments:

Reviewer #2 (Remarks to the Author):

I agreed with the argument in the response "This experimental observation clearly rules out the formation of simple conjugates composed of two "blocks", i.e. in our case, nanoparticles only linked by the end-alkyne terminal groups of the polymer. " It did not form a 'diblock" conjugate, but they are hairy nanoparticles with PLBG as the corona. The difference is that PLBG had rod-like conformation, while the polymers in previous studies might form random coils. I suggested the authors acknowledging previous works on nanoparticle-polymer conjugates in the revised version.

The review suggested by Reviewer #2 in the previous comments has been added [Mei, S., Staub, M. & Li, C. Y. Directed Nanoparticle Assembly through Polymer Crystallization. *Chem. – Eur. J.* **26**, 349–361 (2020).], as well as another recent one [Yi, C., Yang, Y., Liu, B., He, J. & Nie, Z. Polymer-guided assembly of inorganic nanoparticles. *Chem. Soc. Rev.* **49**, 465–508 (2020).]. They are now refs 2 and 3 in the new version of the manuscript.

Reviewer #3 (Remarks to the Author):

The authors have performed additional experiments and addressed the comments raised by the reviewers. The revised manuscript is now suitable for publication in Nature Communications as is.